https://doi.org/10.5194/egusphere-2026-48
Preprint. Discussion started: 13 February 2026

Impact of Ice Microphysical Assumptions on RTTOV Simulations of MSG/SEVIRI Visible and Infrared observations Using W-Band radar Retrieved IWC

Romain JOSEPH[1], Jérôme VIDOT[1], Julien DELANOE[2], and Emmanuel FONTAINE[1]

[1]Météo-France, CNRS, Univ. Toulouse, CNRM, Centre d'Études en Météorologie Satellitaire, Lannion, France
[2]LATMOS/IPSL, UVSQ Université Paris-Saclay, Sorbonne Université, CNRS, Guyancourt, France

Correspondence: Romain JOSEPH (romain.joseph@meteo.fr)

Abstract. This study investigates the impact of ice crystal optical properties on the simulation of radiances associated with a mature deep convective cloud during the west African monsoon, as observed during an airborne case (in visible and infrared) by a geostationary satellite. We performed several simulations for MSG2/SEVIRI channels with the radiative transfer model RTTOV. In these simulations, we used different assumptions in order to test the sensitivity of our simulations to the parameters that are usually used to define the ice cloud properties in models, i.e., size distributions, mass-size relations of ice crystals, and ice crystal shape distributions, where for all these simulations, the ice water content profiles are the same. The ice water content profiles were retrieved using a cloud radar at 94 GHz during an airborne campaign dedicated to the observation of deep convective clouds: Megha-Tropiques in 2010. Simulated radiance for one flight during this campaign are compared to the ones observed by SEVIRI onboard the geostationary satellite MSG2. These simulations allowed us to observed the effect of the sensitivity of the radar reflectivity that can lead to miss informations at the top in deep convective clouds. However, the missing information seems mandatory to explain and reproduce the observed radiance. With the help of additional simulations carried with various amount of ice water content on the top of the cloud and their related ice water path, we are concluding that the most important microphysical parameters to simulate deep convective cloud radiances are the size distributions (especially concentration of small ice hydrometeors) and the distributions of ice water content at their tops. These conclusions are valid for most of the SEVIRI infrared channels and two of its visible channels. However, this study failed to simulate accurately the 1.6 μm and 3.9 μm channels. Hence, the necessary knowledge on condition to perform simulations with these two channels stay an open question.

1 Introduction

Clouds are a central component of the Earth's climate system, regulating the energy balance by reflecting incoming solar radiation and trapping outgoing thermal radiation (Masson-Delmotte et al., 2021). Besides their role in climate, clouds are also a key element in meteorology and weather forecasting, particularly in now-casting, as their rapid evolution strongly influences precipitation and local atmospheric conditions (Zhu et al., 2025; Dolinar et al., 2024). Clouds cover approximately 60-70% of the Earth's surface, of which 40-50% are high-level clouds (Stubenrauch et al., 2013). The fraction of high clouds is particularly

https://doi.org/10.5194/egusphere-2026-48
Preprint. Discussion started: 13 February 2026

large in the Tropics (Wylie and Menzel, 1999), where deep convection frequently produces extensive cirrus and anvils. And significant proportion of these clouds (about 40%) are composed primarily of ice particles (Massie et al., 2002). Ice clouds play a particularly important role, as they occur frequently at high altitudes and exert a strong influence on both short- and long-wave radiative fluxes (Liou, 1986). Despite decades of research, their microphysical and optical properties remain an active area of research, which limits our ability to represent them accurately in both climate models (Bony et al., 2015) and weather prediction systems (Geer et al.).

One of the main challenges arises from the complexity of ice crystal shapes and their size distributions, which are difficult to observe directly, hence to represent accurately in models. Even the vertical distribution of cloud ice mass is still poorly constrained by satellite products and reanalyses for tropical clouds (Duncan and Eriksson, 2018). Satellite retrieval algorithms can provide estimates of cloud-top pressure, optical thickness, or effective radius, but these depend strongly on the retrieval approach often leading to significant discrepancies in the tropics (Hamann et al., 2014). As a result, the assimilation of cloudy infrared radiances into numerical weather prediction (NWP) systems remains very limited: operational NWP centers still rely almost exclusively on clear-sky radiances. There is still work to be done on cloudy sky, where radiances from cold high-level ice clouds ($T < 230$ K) cannot be represented (Okamoto et al., 2023).

Radiative transfer (RT) models play a central role in this context, since they are the link between cloud microphysical properties and satellite measurements. They are the foundation both for satellite retrieval algorithms (inversion) and for the assimilation of radiances in NWP. RTTOV (Radiative Transfer for TOVs), in particular, is widely used in operational centers as a fast RT model (Saunders et al., 2018). However, its built-in parametrizations of ice optical properties (Baum et al., 2011; Baran et al., 2014; Vidot et al., 2015) rely on validity ranges and simplified representations of ice particle habit. The use of external optical property databases (Yang et al., 2013) allows for a more explicit treatment of ice particle morphology and spectral variability, but their impact on simulated radiances remains insufficiently explored.

The objective of this study is therefore to evaluate how different representations of ice microphysics affect radiative transfer simulations of tropical convective clouds. Using in situ Ice Water Content (IWC) profiles from the RASTA radar (W-band at 94 GHz) during the MeghaTropiques campaign (Roca et al., 2015), we perform RTTOV simulations with both standard and newly developed optical property schemes, including sensitivity tests to cloud-top IWC. The simulations aim to reproduce the SEVIRI observations from the Meteosat Second Generation (MSG) geostationary satellites. SEVIRI is a multispectral imager operating in the visible and infrared spectral regions. We aim to identify the key factors controlling RT in deep convective clouds and to assess their implications for the assimilation and inversion of satellite radiances.

Specifically, this work addresses three main questions:

1. How can current RTTOV schemes reproduce observed SEVIRI radiances in tropical deep convection?
2. How sensitive are radiative transfer simulations to explicit representations of ice particle habit, number, shapes and density?
3. How does the representation of cloud-top ice influence the accuracy of infrared and visible radiative transfer simulations?

https://doi.org/10.5194/egusphere-2026-48
Preprint. Discussion started: 13 February 2026

By focusing on these questions, the study highlights the importance of radiative transfer in constraining cloud properties, and provides insights that are directly relevant for the assimilation of geostationary radiances and the development of improved retrieval algorithms for convective systems in the tropics.

To address these questions, the paper is organized as follows. First, we present the datasets used in this study. Then we describe the methodology developed to link these datasets to Yang et al. (2013) database and to derive new optical properties. These newly derived optical properties, together with those implemented in RTTOV, are subsequently used to simulate MSG/SEVIRI observations and to analyse the differences between the various approaches. The last section present and discuss the results and their impact on radiative transfer in this case. Rather than aiming at a statistical characterization of deep convection, this study adopts a case-study approach to examine the radiative impact of a specific convective cloud system with a well-defined vertical structure.

2 Methods

To study the sensitivity of RTTOV simulations to the optical properties of ice clouds, we combine ERA5 reanalysis of atmospheric profiles with IWC profiles retrieved from in-situ observations. These data are used to derive optical properties and simulate brightness temperatures using the RTTOV radiative transfer model (version 13.2).

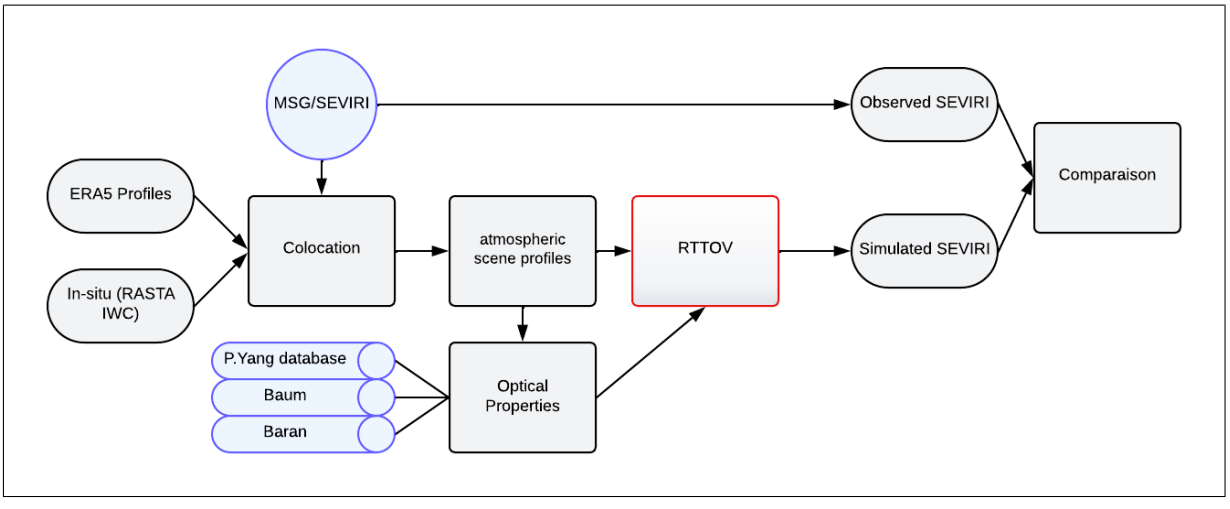

Figure 1. Schematic representation of the processing steps from the in-situ measurement with ERA5 profiles to the comparison of radiances between RTTOV simulations and satellite observations

This diagram 1 shows the logic of the processing and their link with the data used in this study. The first section introduces the data and the Megha-Tropiques campaign, which provide the foundation for constructing the atmospheric profiles employed in the simulations (Section 2.1). These datasets are co-located with observations from the geostationary satellite MSG2/SEVIRI (Schmetz et al., 2002) to construct consistent atmospheric scene profiles (Section 2.1.2). In parallel, the optical properties of ice particles are taken from the database Yang et al. (2013) (Section 2.2.2). This database will be used to determine optical

https://doi.org/10.5194/egusphere-2026-48
Preprint. Discussion started: 13 February 2026

properties according to different crystal shapes in order to perform simulations. In addition to modifying the shape, we will seek to modify the particle size distribution. In order to test the impact of shape and concentration on these optical properties. Both the atmospheric scene profiles and the optical properties are then used as inputs to RTTOV, which generates simulated SEVIRI radiances. Whether it be the new optical properties developed for this paper or those offered with parametrization in RTTOV. These simulated radiances are finally compared with the observed ones from MSG/SEVIRI radiances (Section 3). All the elements of this figure 1 are present, summarising how the comparison of radiances between simulations and observations is carried out based on in-situ measurements from the IWC.

2.1 Overview of the Observational Data Sets

2.1.1 Airborne in-situ observations

The Megha-Tropiques airborne measurement campaign took place in August 2010 on board SAFIRE's Falcon 20 and was based in Niamey (Niger) (Roca et al., 2015). This field campaign was designed in the framework of the Megha-Tropiques satellite mission, with the objective of providing dedicated in-situ from airborne measurements for the validation of satellite retrievals in tropical cloud systems. The flights were mainly conducted in the stratiform region of mesoscale convective systems, where large ice cloud offer favourable conditions for evaluating satellite-based retrieval algorithms.

The aircraft was equipped with several instruments, including a W-band Doppler radar at 94 GHz called RASTA (Protat et al., 2009; Delanoë et al., 2014), which is mainly used for this study. Among the 11 flights performed during the campaign, we will focus on the flight 17 performed the 10/08/2010 between 08:45 and 11:30 UTC. RASTA provided observations of the reflectivity of ice clouds and enables the derivation of vertical profiles of the IWC, using the variational approach described in Delanoë and Hogan (2008). In addition, the airborne observations were complemented by ground-based radar (C band and X band) measurements over Niamey, providing a comprehensive dataset to characterize the vertical structure of tropical convective systems (Drigeard et al., 2015).

Uncertainties on the retrieval of IWC are describe in (Delanoë et al., 2014) and (Protat et al., 2019). Also, previous studies have quantified that mass-diameter relationships can introduce IWC uncertainties on the order of a factor of two (Fridlind et al., 2015).

As shown in figure 2, the aircraft flew into the stratiform part of a large deep convective system (in blue in the figure), with mostly IWC larger than 0.1 $\mathrm{g\,m^{-3}}$ (Fontaine et al., 2020). In this case, the brightness temperatures observed by MSG2/SEVIRI in the 10.8 μm channel are a good indicator of the temperature at the top of the cloud. Mostly, the aircraft flew in the part of the cloud where cloud tops are in the range [200K ; 220K]. The different observation time steps are labeled from (a) to (f) (Fig 2a) and delimit the IWC profiles in Figure 2b.

https://doi.org/10.5194/egusphere-2026-48
Preprint. Discussion started: 13 February 2026

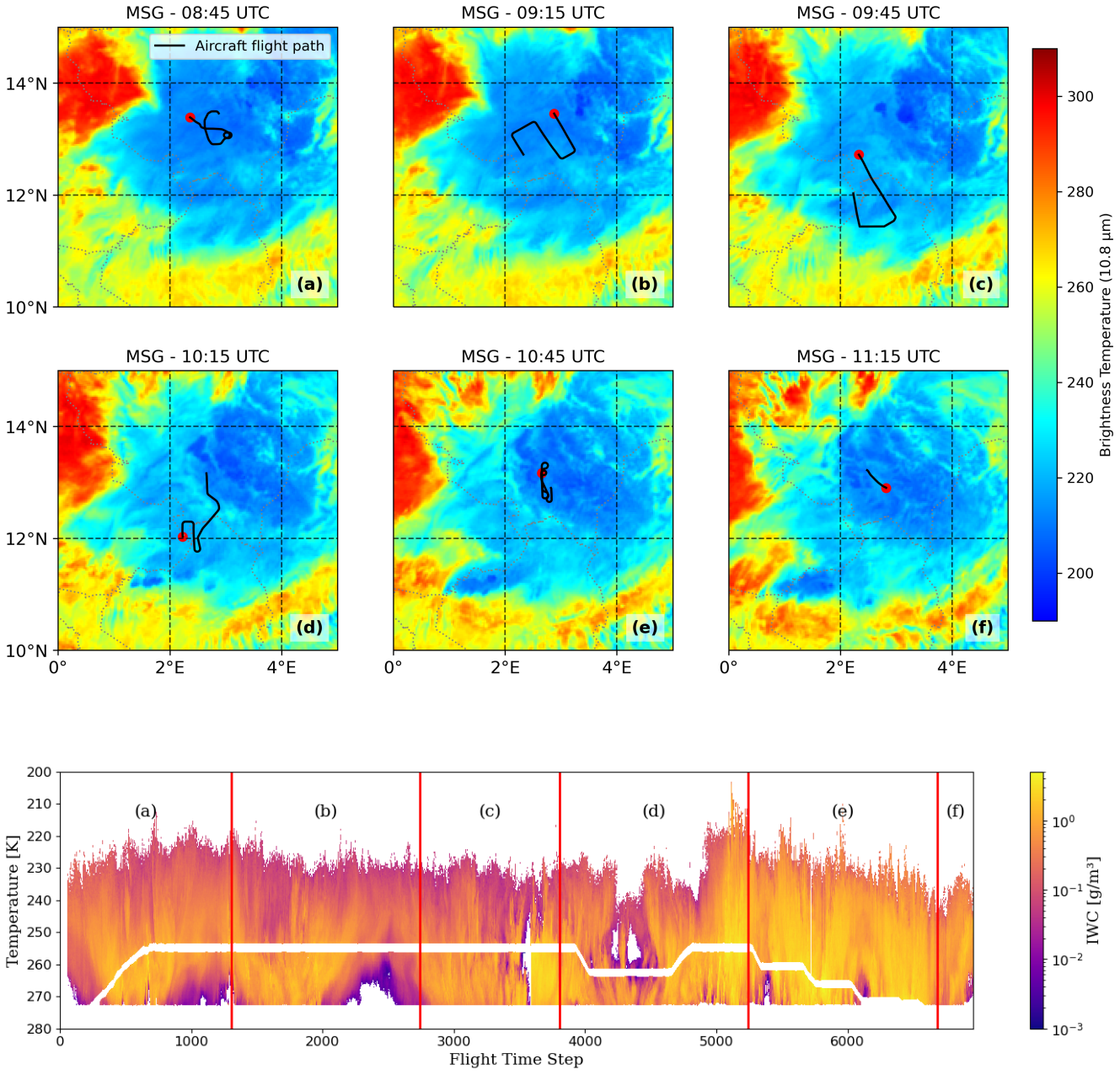

Figure 2. (Upper panel) SEVIRI imager observations onboard Meteosat Second Generation 2 during flight 17, divided into six sections (a–f) corresponding to different satellite time steps. The colour scale represents the brightness temperature at 10.8 μm. Black lines indicate the flight tracks for each period, and the red dot marks the starting point. (Lower panel) Ice water content profiles retrieved from cloud radar (colour scale, in $\mathrm{g\,m^{-3}}$) combined with ERA5 temperature on the y-axis and flight time steps on the x-axis (one time step corresponds to approximately 1.6 s). Flight 17 of the Megha-Tropiques campaign.

https://doi.org/10.5194/egusphere-2026-48
Preprint. Discussion started: 13 February 2026

Figure 2 shows the profile of the retrieved IWC based on the reflectivity measured by RASTA. The aircraft track is visible with its footprint in white in the colorplot. Variability of IWC is higher in the profiles from zones (a) to (d) than in zones (e) and (f): with IWC ranging from 10^{-3} g m^{-3} to 1 g m^{-3} against IWC in the range [10^{-2} g m^{-3} : 5 g m^{-3}]. In the zones (e) and (f), the aircraft is located in the coldest part of the convective system (Figure 2) displays high IWC larger than 2 g m^{-3}. However, in this area, IWC profiles do not reach higher altitudes than at the beginning of the flight. These parts highlight radar attenuation at the top of the cloud (Pujol et al., 2007).

2.1.2 Co-location of Airborne and Satellite Observations

MSG/SEVIRI has a spatial resolution of 3 km at nadir with a temporal sampling period of 15 min. Temporally and spatially, the resolutions between airborne measurements and satellite observations are different. In order to be able to simulate the satellite observations and compare the radiance, our in-situ observations need to be re-gridded on MSG grid.

Then, in-situ measurements within a pixel are averaged to obtain the average IWC profile per pixel, as shown in figure 3. In addition, each profile is associated with the MSG scan with the closest time. The maximum temporal mismatch is therefore limited to $\pm$7.5 min, which may still be significant in convective condition, but represents a reasonable compromise for the comparison (Hamann et al., 2014). Know that previous studies showed that 10 minutes of time difference can lead to substantial discrepancies in cloud-state validation metrics (Bojanowski et al., 2014), which suggests that corresponding radiance values may differ by several kelvins in infrared window channels. For flight 17, the number of points is reduced from 6957 time steps to 578.

Retrieved IWC profiles can reach up 15 km above and below the plane, discretized over 500 levels with a pixel resolution of 60 meters (Fig 2). Figure 3 shows IWC profiles interpolated on the model levels of ERA5, where a linear interpolation is applied. Hence, IWC profiles are re-gridded onto the MSG grid using a nearest-neighbour approach in latitude–longitude space. This strategy adopted here, based on pixel averaging and temporal matching, was used in former satellite–airborne comparison studies (Rädel et al., 2008; Hamann et al., 2014). Although uncertainties remain due to temporal mismatch and pixel-scale heterogeneity.

https://doi.org/10.5194/egusphere-2026-48
Preprint. Discussion started: 13 February 2026

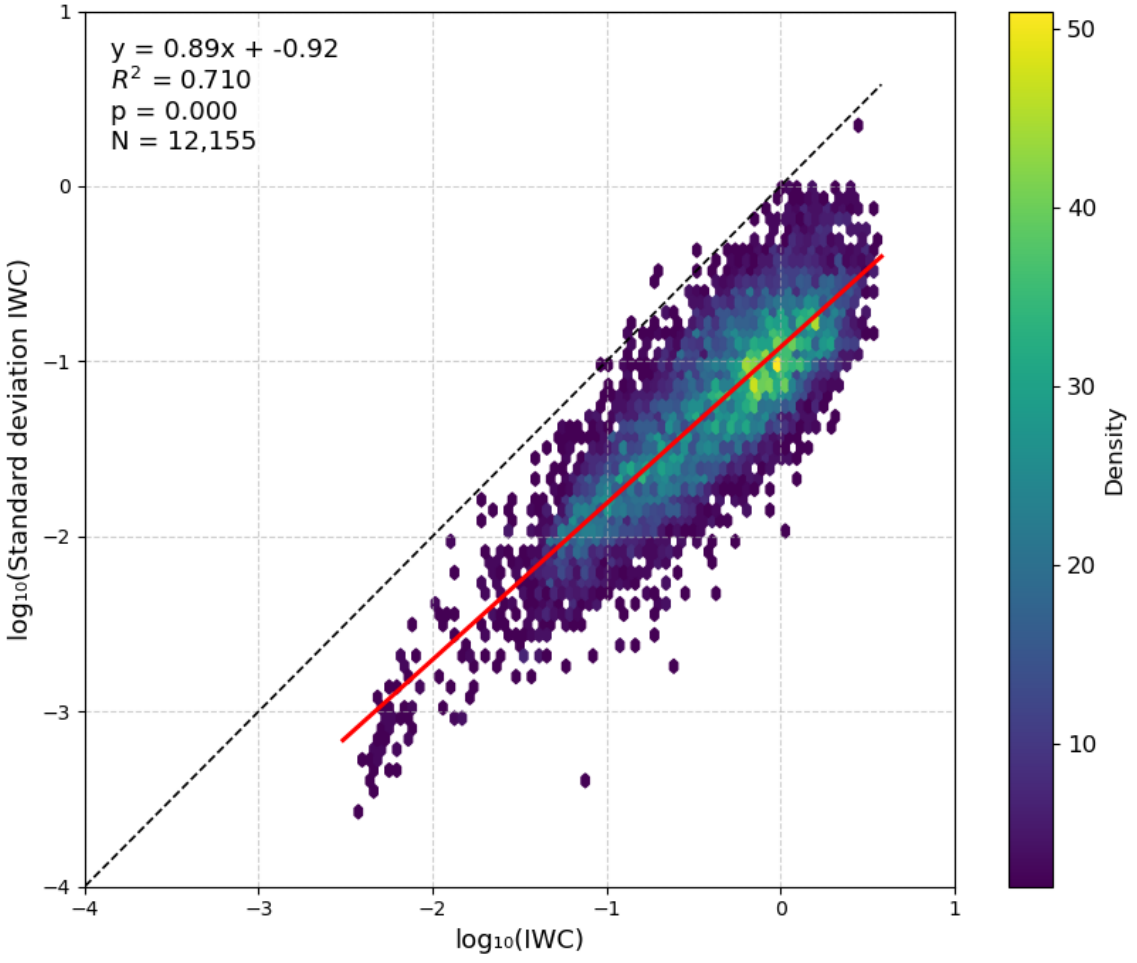

Figure 3. Correlation between the standard deviation [g m^{-3}] within MSG pixels in function of Ice water content [g m^{-3}]

The variability of IWC in one pixel of the MSG grid is given by the standard deviation of IWC in figure 3. Where, IWC standard deviation tend to be larger with larger IWC. Indeed, the standard deviation reach 1 g m^{-3} in the last part of the flight. A correlation with an R^2 value of 0.7 is therefore observed between the standard deviation and the IWC. This standard deviation appears to be around 10%, which is relatively negligible compared to the measurement uncertainties.

2.1.3 Case description and vertical structure

Figure 4 presents the vertical profiles of temperature, specific humidity, ice water content. The IWC profiles are retrieved from the RASTA W-band radar observations, while temperature and humidity profiles are taken from the co-located ERA5 reanalysis. Liquid water content is not available from in situ measurements and is therefore estimated from ERA5. Indeed, this campaign primarily focuses on the ice phase of clouds in deep convective systems.

https://doi.org/10.5194/egusphere-2026-48
Preprint. Discussion started: 13 February 2026

Since LWC is not retrieved from the RASTA observations, a sensitivity experiment was performed to evaluate the impact of liquid water. Two LWC profiles derived from ERA5 for the flight region and time period were considered : a median LWC profile and a high-LWC profile. The results show that, for this specific case, the influence of LWC on SEVIRI observations is not significant. Consequently, LWC was not included in the reference simulations.

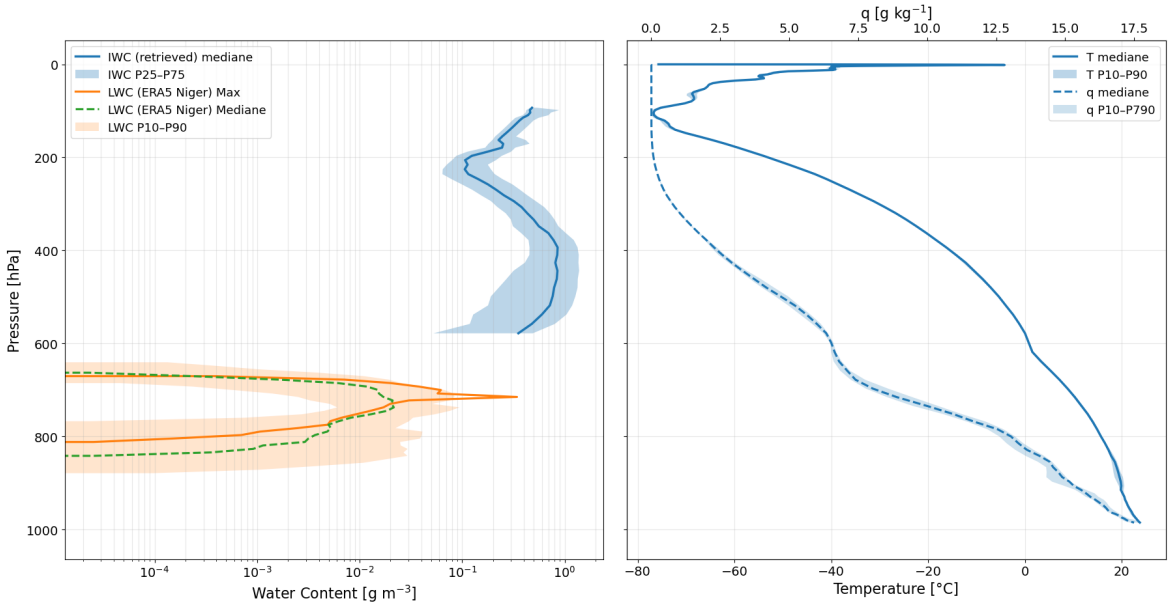

Figure 4. Vertical profiles of ice water content (IWC), liquid water content (LWC), temperature, and specific humidity characterizing the analyzed convective cloud system. IWC profiles are retrieved from RASTA radar observations, while temperature, humidity, and LWC are derived from ERA5 reanalysis. Solid lines indicate median profiles and shaded areas represent the interquartile range (P10–P90).

The vertical profiles highlight a cloud system characterized by a large amount of ice water content at high altitudes, indicative of an extensive anvil cloud. The ice phase clearly dominates the upper troposphere, while liquid water content remains weak and confined to a limited altitude range in the ERA5-derived profiles.

Such a vertical structure is not fully representative of an actively developing deep convective cloud, in which a more substantial liquid water layer is typically expected. Instead, the analysed scene corresponds to a particular case dominated by ice in the upper levels, consistent with a mature or decaying stage of a convective system.

It is important to emphasize that the conclusions drawn in this study are specific to this single case and to cloud systems exhibiting similar vertical structures. They should not be interpreted as representative of all deep convective clouds.

https://doi.org/10.5194/egusphere-2026-48
Preprint. Discussion started: 13 February 2026

2.2 Specification of Optical Properties

2.2.1 Ice particle Habits

For ice clouds, RTTOV provides two internal parametrization of the optical properties to perform RT simulation in visible and infrared. The first is Baum's parametrization (Baum et al., 2011), which relates the effective diameter of the ice particles to temperature and IWC. This effective diameter will be used to read a look-up table and provide the optical properties. RTTOV proposes four different settings to compute the effective diameter. In this study, we focus on two of them: the one developed by Wyser (1998) (W98), recommended in RTTOV and designed to represent large-scale clouds and the one developed by McFarquhar et al. (2003) (MF03) and derived from observations of cirrus generated by deep tropical convection. The second option in RTTOV is Baran's parametrization (Baran et al., 2014; Vidot et al., 2015), which introduces a self-consistent framework where the optical properties depends explicitly on IWC and temperature. These schemes have been developed and tuned against in-situ measurements and satellite retrievals, and are now standard options in RTTOV. Both methods assume a fixed particle habit i.e. the distribution of the different types of ice crystals stay the same as function of IWC and T.

However, RTTOV also enables simulations to be performed using externally defined optical properties, thus avoiding reliance on internal parametrizations. In this study, we explore this alternative approach by using the spectrally-resolved database of ice optical properties developed by Yang et al. (2013). This database is widely used in the atmospheric science community (Baum et al., 2014; Cole et al., 2014; Wang et al., 2016; Baek et al., 2018), as it provides single-scattering properties for nine different ice crystal habits, covering the spectral domain from 0.2 μm to 100 μm and particle diameters ranging from 2 μm to 10 mm.

The database contains both pristine ice crystals (droxtal, column, plate, bullet rosette) and more complex ice aggregates (snow) (clusters of plates or columns). These morphological differences are known to significantly affect scattering and absorption, and in particular the angular distribution of scattered radiation, i.e. the phase function (Key et al., 2002).

To connect the retrieved IWC profiles to this database, we define three distinct methods. All three approaches share the same starting point: a mass–diameter relationship obtained from tropical convective systems (Fontaine et al., 2020), together with a particle size distribution based on Field et al. (2007). This ensures that the representation of particle populations is constrained with tropical convective environment parametrization.

The three methods differ in how they associate particle shapes with the mass–diameter law:

https://doi.org/10.5194/egusphere-2026-48
Preprint. Discussion started: 13 February 2026

Method	Description
Method 1 and Method 1-bis	For each diameter, the particle with the closest mass–diameter relationship to Fontaine et al. (2020) is selected.
Method 2	For each diameter, a combination of two shapes is selected, framing the mass–diameter relationship (one above and one below).
Method 3	Identical to Method 2, except that pristine and snow crystals are distinguished. When the diameter is less than 150 μm → Pristine; if greater → Snow. (Schmitt and Heymsfield, 2014)

Table 1. Description of the different methods used to select the ice particle habit.

The three approaches were designed to test the sensitivity of simulated radiance to the complexity of ice particle morphology. As described in Table 1, for each diameter we identify either a single ice crystal habit (Method 1) or two ice crystal habits (Methods 2 and 3) whose mass–diameter relationships are the closest to the selected reference relationship (Fontaine et al., 2020). This first step therefore aims at determining which particle shape best matches the expected particle mass for a given diameter. At this stage, the ice particle habit is defined by selecting one or two representative crystal shapes for each diameter. Method 1 represents the simplest approximation, where only the closest mass–diameter relationship is retained. Method 1-bis is identical to Method 1 except for the choice of the particle size distribution; it therefore represents an alternative formulation of Method 1, hence the designation '1-bis'. Once the ice crystal shapes have been determined, their concentrations must be specified. These particle size distribution parametrizations are discussed in the following section 2.2.2. Methods 2 and 3 progressively increase complexity by introducing mixtures of particle habits and distinguishing between pristine and snow. Note that method 3 uses a diameter threshold of 150 μm to help distinguish between pristine ice and aggregated ones. We are aware that the distinction between pristine ice and snow aggregates is more complex (Schmitt et al., 2016), but to simplify our study we choose the threshold of 150 μm that seems a good compromised taking the results from (Schmitt et al., 2016).

Thus, for each temperature and diameter, a choice of shape will be determined based on the mass-diameter relationship among the nine shapes presented in Yang et al. (2013). Indeed, the mass–diameter relationship used in this study varies with temperature. An example for the method 1 at 210 K is displayed in figure 5.

https://doi.org/10.5194/egusphere-2026-48
Preprint. Discussion started: 13 February 2026

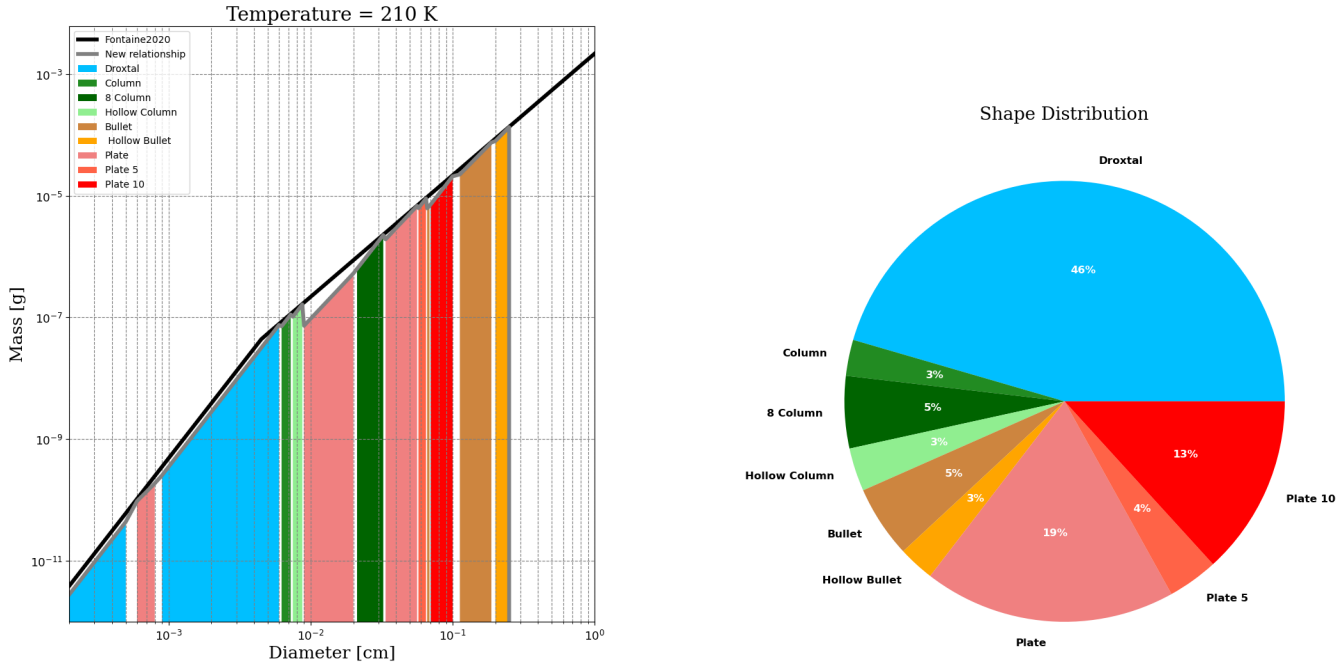

(a) (b)

Figure 5. Example of Ice Particle Habit following the Method 1 at 210 K. (a) represent the mass-diameter relationship of Fontaine et al. (2020) at 210 K and the shape selection as function of the diameter. (b) the contribution in percent of each shape retrieved by method 1.

190 In this figure 5, we can notice that smallest diameters are mainly droxtal type (quasi-spherical shape). For larger diameters, more complex shapes appear, such as simple plates and aggregates. Figure 6 illustrate the fact that the combination of shapes vary with the temperatures and the method (1,2 and 3).

https://doi.org/10.5194/egusphere-2026-48
Preprint. Discussion started: 13 February 2026

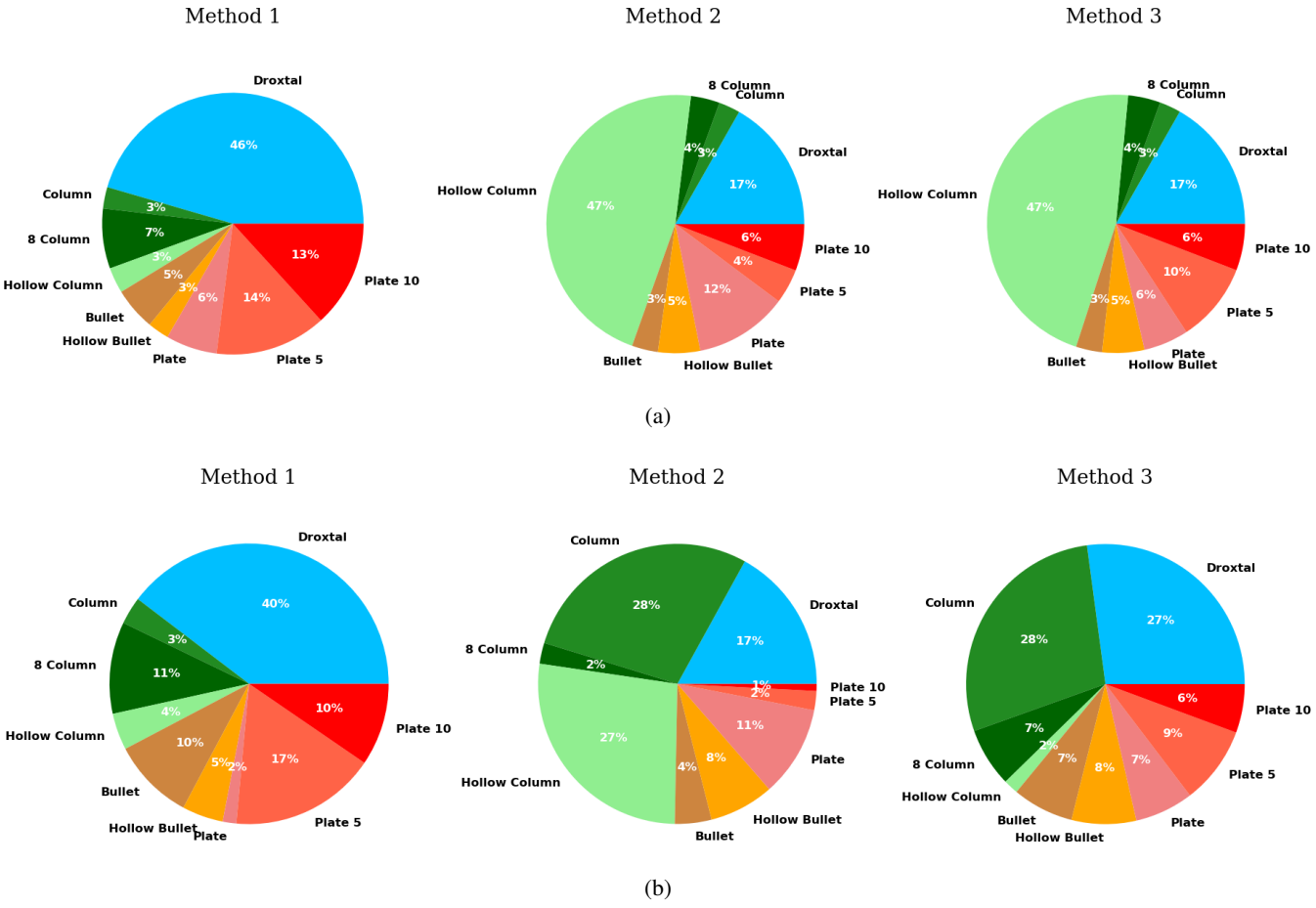

Figure 6. Distribution of ice particle shapes for the three different methods. (a) Results at 210 K and (b) at 230 K.

At 210 K, Methods 2 and 3 select the same ice crystal habits, as they are mainly dominated with pristine ice. With nearly 50 % of hollow columns, this habit is the most frequent at this temperature. Droxtal represent only 17 % for these two methods, which is significantly lower than the 46% obtained with Method 1. When the temperature increases to 230 K, differences between Methods 2 and 3 start to appear. Ice crystals habit from Method 3 includes more complex crystal shapes and the proportion of hollow columns decreases from 27 % to 2 %. It allows an increase of aggregated particles such as aggregates of 10 Plates (from 1 %to 6 %) and aggregates of 8 Columns (from 2 % to 7 %).

Once the particle shapes distributions are assigned, the bulk optical properties of each cloud layer are calculated. RTTOV requires three quantities to simulate radiance: the absorption coefficient σ_{abs}, the scattering coefficient σ_{sca}, and the phase function $P(\theta)$. Because radiative transfer operates at the scale of a satellite pixel or an atmospheric layer, the single-particle optical properties from Yang et al. (2013) must be integrated over the particle size distribution (PSD) and weighted by the occurrence of each habit. This aggregation yields "bulk" coefficients representative of the ensemble of particles present in the layer. Equations to compute the bulk properties are as followed Baum et al. (2005):

https://doi.org/10.5194/egusphere-2026-48
Preprint. Discussion started: 13 February 2026

$$\sigma_{sca/abs} = \frac{\int_{\lambda_1}^{\lambda_2}\int_{Dmin}^{Dmax}\left[\sum_{h=1}^{M}\sigma_{sca/abs,h}(D,\lambda)f_h(D)\right]n(D)F_s(\lambda)S(\lambda)dD}{\int_{\lambda_1}^{\lambda_2}\int_{Dmin}^{Dmax}\left[\sum_{h=1}^{M}f_h(D)\right]n(D)F_s(\lambda)S(\lambda)dD} \quad (1)$$

$$P(\theta) = \frac{\int_{\lambda_1}^{\lambda_2}\int_{Dmin}^{Dmax}\left[\sum_{h=1}^{M}P_h(\theta,D,\lambda)\sigma_{sca,h}(D,\lambda)f_h(D)\right]n(D)F_s(\lambda)S(\lambda)dD}{\int_{\lambda_1}^{\lambda_2}\int_{Dmin}^{Dmax}\left[\sum_{h=1}^{M}\sigma_{sca,h}(D,\lambda)f_h(D)\right]n(D)F_s(\lambda)S(\lambda)dD} \quad (2)$$

with σ the scattering or absorption coefficient (m^{-1}), f_h the fraction of the particle of shape h, $n(D)$ the particle size distribution of size D (mm), $S(\lambda)$ the solar spectrum (W m^{-2} μm^{-1}), and $F_s(\lambda)$ the spectral response function. In the infrared, the solar spectrum is replaced by the Planck function $B(\lambda)$ from an opaque ice cloud at 233 K.

These formulations ensure that the simulated bulk optical properties are representative of the entire particle population, weighted consistently by the particle size distribution and the spectral response function of the channel of the instrument.

2.2.2 Optical Properties Schemes

As discussed in Section 2.2.1, RTTOV currently implements two parametrization schemes to derive the optical properties of ice clouds. Both require the IWC and temperature (T) profiles as inputs to retrieve these properties from pre-computed look-up tables. Table 2 summarizes the differences between the two RTTOV schemes and the new methods proposed in this study:

Table 2. Overview of the schemes used to determine ice optical properties in order to make the RTTOV simulation.

Scheme	**mass-Diameter relationship**	**PSD**	**Ice habit**	**Scattering methods**
Baran	(Cotton et al., 2013)	(Field et al., 2007)	Fixed	T-matrix + geometric optics
Baum (W98 and MF03)	(Yang et al., 2013)	Gamma law	Fixed	Discrete dipole approximation + geometric optics
Method 1–2–3	(Fontaine et al., 2020)	(Fontaine et al., 2020)	Varying with T	Discrete dipole approximation + geometric optics
Method 1 bis	(Fontaine et al., 2020)	(Field et al., 2007)	Varying with T	Discrete dipole approximation + geometric optics

The primary distinction between the RTTOV schemes and the newly proposed methods lies in the representation of ice crystal shapes, which in the latter vary as a function of temperature. Note that at 210 K the mass-size distributions of Cotton

https://doi.org/10.5194/egusphere-2026-48
Preprint. Discussion started: 13 February 2026

et al. (2013) and Fontaine et al. (2020) are similar. The objective of this study is to assess how the choice of crystal shape influences the simulation of satellite radiance. This comparison highlights that the newly proposed methods differ from the RTTOV parametrizations not only in their choice of size distribution, but also in their explicit dependence on particle shape and temperature. The differences between the four new methods arise from two main aspects: particle shape and particle size distribution (PSD). Methods 1, 2, and 3 are designed to highlight the sensitivity of the results to the choice of particle habit, with Method 3 constraining the representation to more complex shapes. By contrast, the distinction between Method 1 and Method 1-bis lies in the assumed PSD. Owing to the use of two different PSDs, Method 1 yields a larger proportion of small particles compared with Method 1-bis (Fontaine et al., 2020).

Both RTTOV parametrizations have validity ranges with respect to IWC. For Baran's scheme, the IWC must remain between 6.0×10^{-6} g/m^3 and 1.97 g/m^3. For Baum, the valid range is between 4.98×10^{-5} g/m^3 and 0.18 g/m^3. It is important to notice that the limit of IWC for Baum, will be only take into account for the parametrization of the effective diameter. But not for the calculation of the optical properties in the parametrization. Figure 7 shows the distribution of IWC values retrieved from the airborne profiles compared with these limits.

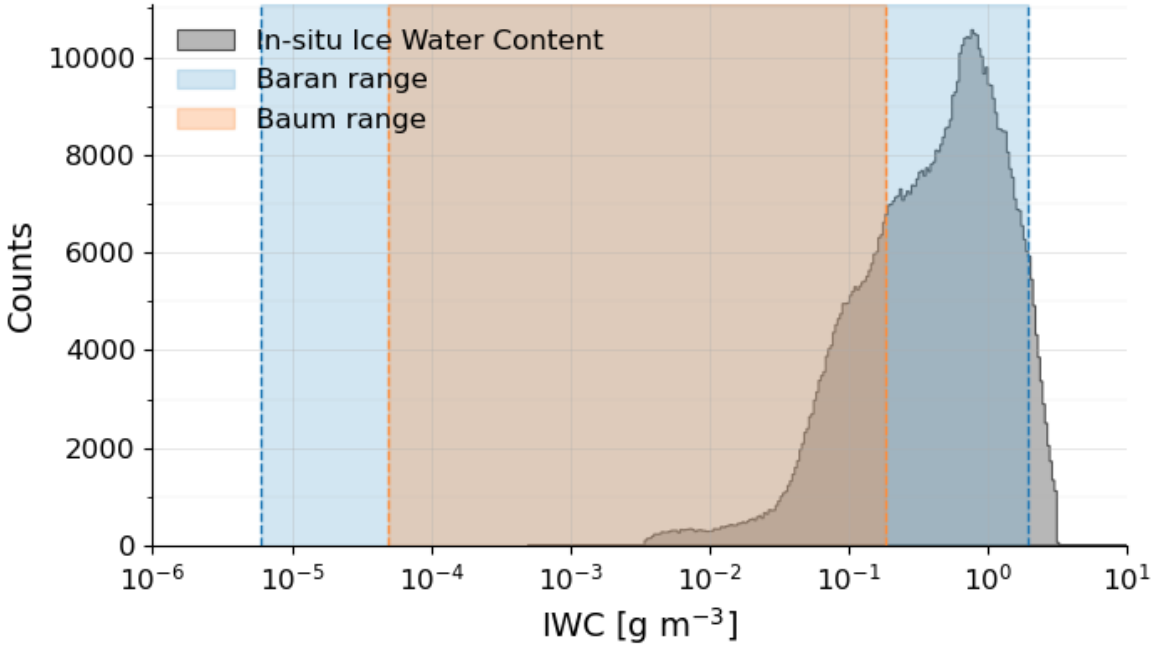

Figure 7. Distribution of retrieved IWC in [g/m^3] compared to the validity ranges of the RTTOV parametrizations.

For both parametrizations of RTTOV the distribution of retrieved IWC is not totally covered by their limits, especially high IWC (IWC> 1 g m^{-3}). It is important to note that the Baum parametrization upper limit does not allow to cover with consistency 73% of the dataset. IWC often exceed the maximum thresholds considered by RTTOV. In tropical mesoscale

https://doi.org/10.5194/egusphere-2026-48
Preprint. Discussion started: 13 February 2026

convective systems (MCSs), the IWC frequently exceeds 1 $\mathrm{g\,m^{-3}}$ (Korolev et al., 2024).In such cases, the IWC is capped to the upper threshold during simulations with RTTOV's built-in schemes. For the Baum parametrization, only 27 % of the values fall within the prescribed limits, compared to 94 % for the Baran scheme.

2.2.3 Extinction coefficient

In this section, we examine the extinction coefficient β_{ext}, which controls the total attenuation by ice particles. It's the summation of both scattering and absorption. Comparing extinction values across different schemes provides insight into how particle habit and size assumptions impact radiative transfer simulations.

This coefficient depends on particle size, shape, concentration, and is therefore a key element of radiative transfer theory (Bohren and Huffman, 1998). Figure 8 shows the differences in extinction coefficients between the three new methods and the RTTOV schemes, for the visible (0.8 μm). These extinction coefficients are plotted as a function of IWC and temperature retrieved during the flight. The colored pixels therefore correspond only to the temperature–IWC combinations sampled by the airborne measurements, although the method could in principle be applied to all possible combinations of temperature and IWC.

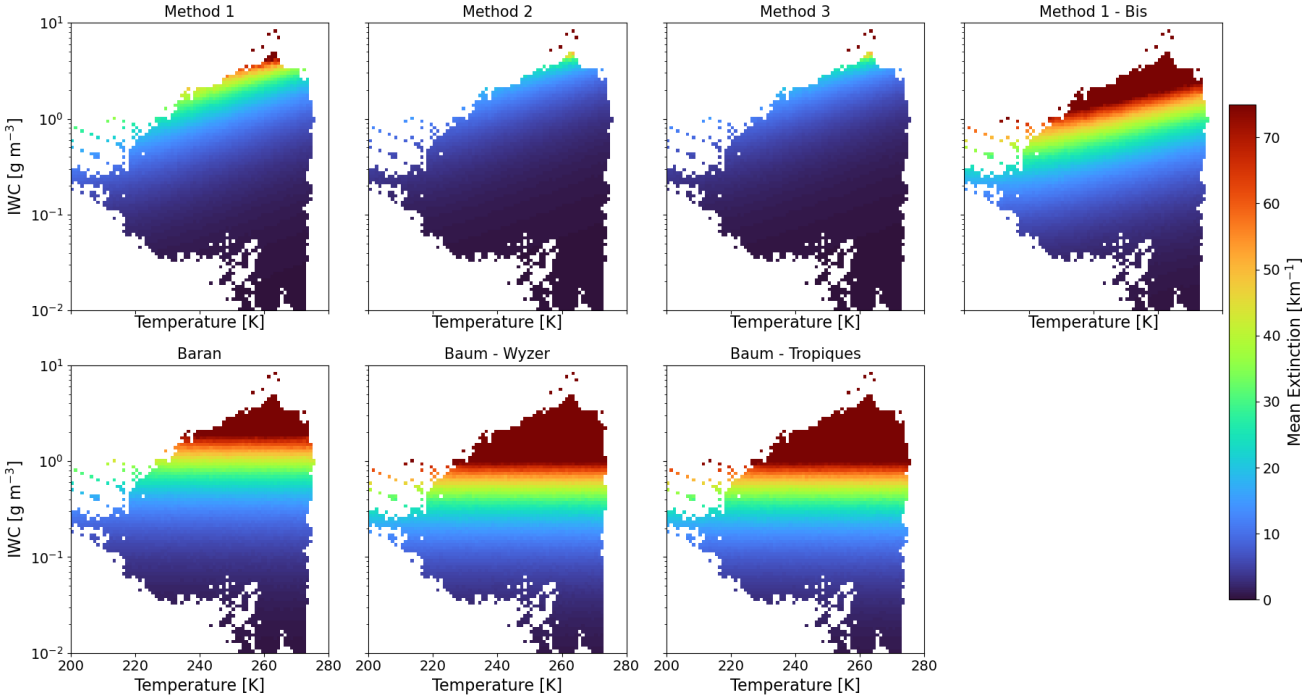

Figure 8. Extinction coefficients for the wavelength of 0.8 μm in function of IWC and T for the new methods and the parametrization of RTTOV

https://doi.org/10.5194/egusphere-2026-48
Preprint. Discussion started: 13 February 2026

Method 1-bis has extinction coefficients in the same order of magnitude as the parametrizations proposed by RTTOV showing that the choice of PSD have more impact than the choice of shapes on the extinction, especially regarding the concentration of small hydrometeors (Method 1 versus Method 1bis). The choice of shape is also important, as there is a difference between method 1 and method 2 which can be explained by the ice particle shape distributions. Method 2 and 3 produce smaller extinction than the other ones. For $T < 220$ K (top of the cloud), The extinction coefficients according to methods 1 and 1-bis, as well as Baum/Baran, are close, implying that attenuation at cloud tops is of comparable magnitude across methods (Method 2 and 3 have smaller coefficients). When the IWC exceeds 0.1 $\mathrm{g\,m^{-3}}$, the extinction coefficient tends to reach values greater than 40 $\mathrm{km^{-1}}$ for each RTTOV method and for Method 1-bis. Thus, beyond a certain ice threshold, this value of extinction becomes particularly important. With our three methods the impact of the temperature for the calculation of the extinction is more important.

The discrepancies between each methods at 0.8 μm suggest the need to better constrain extinction in high-IWC regimes.

2.2.4 Phase function

Next, we consider the phase function, which describes the angular distribution of scattered radiation. This function is especially important in the visible spectrum, where scattering strongly influences satellite-observed reflectance (Liou, 2002; Baran, 2009).

In the infrared, it is mainly used to calculate the backscatter coefficient.

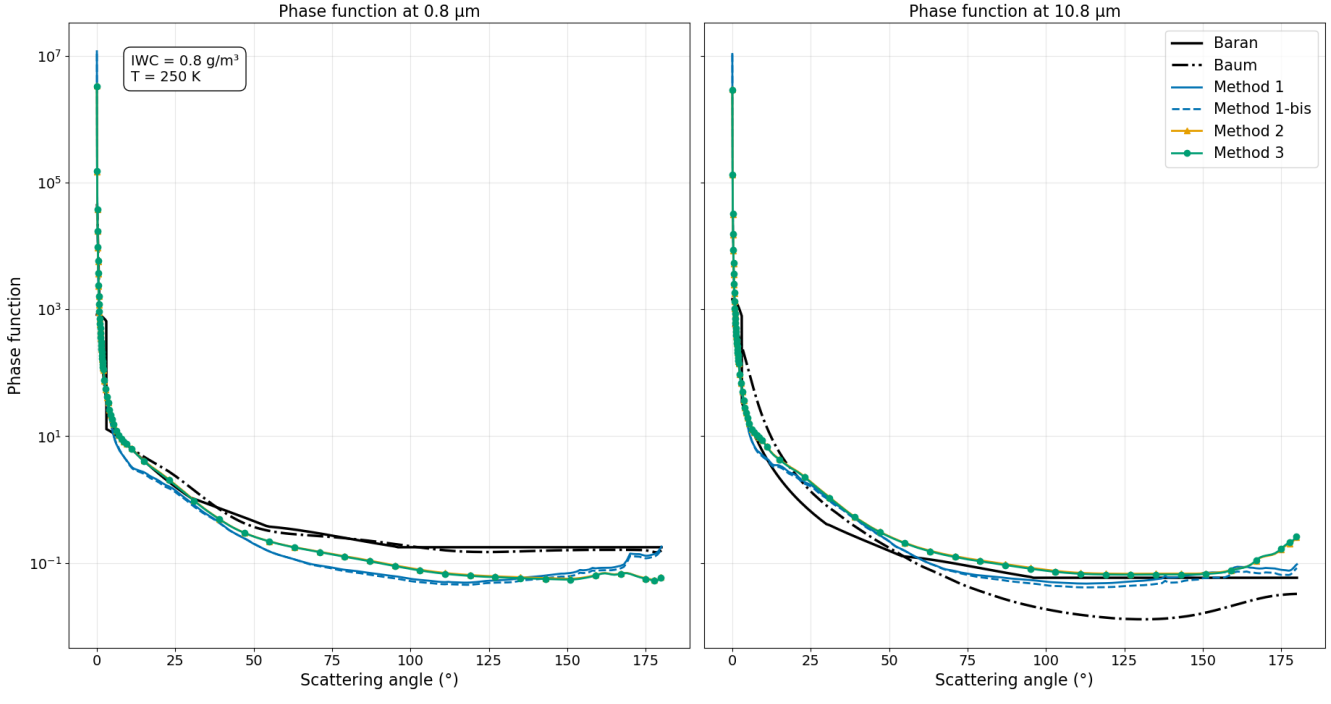

Figure 9. Comparison of phase functions between the new methods and RTTOV parametrizations (Baum W98 and Baran). In the left for the visible channel 0.8 μm and in the right for the the infrared channel 10. 8μm. Both at a temperature of 250 K and an IWC of 0.8 g/m^3 .

https://doi.org/10.5194/egusphere-2026-48
Preprint. Discussion started: 13 February 2026

The phase functions highlight strong contrasts between the visible and infrared domains. In the visible (Figure 9), the new methods exhibit very pronounced anisotropy, with a sharper forward peak (scattering angle near 0°) followed by a rapid drop-off beyond 25°, consistent with a scattering regime dominated by large particles (Mishchenko et al., 1996). The two parametrizations from RTTOV methods show broader angular distributions, with higher values sustained between 25° and 180°, indicating enhanced lateral and backward scattering. These differences have a strong potential impact on simulated radiances in the visible range.

In the thermal infrared (Figure 9), by contrast, all methods yield more homogeneous phase functions. A forward peak is still present, but its amplitude is smaller in the visible. Beyond a few degrees, the functions maintain uniformly low values across angles up to 180°, with only a weak backscattering enhancement. At these wavelengths (around 10 μm), absorption dominates over scattering, reducing the sensitivity to crystal geometry and leading to a more uniform angular response.

All these phase functions exhibit a pronounced forward-scattering peak, which is directly reflected in the value of the corresponding asymmetry parameter. The asymmetry parameter represents the mean cosine of the scattering angle, providing a measure of the preferential direction of scattering.

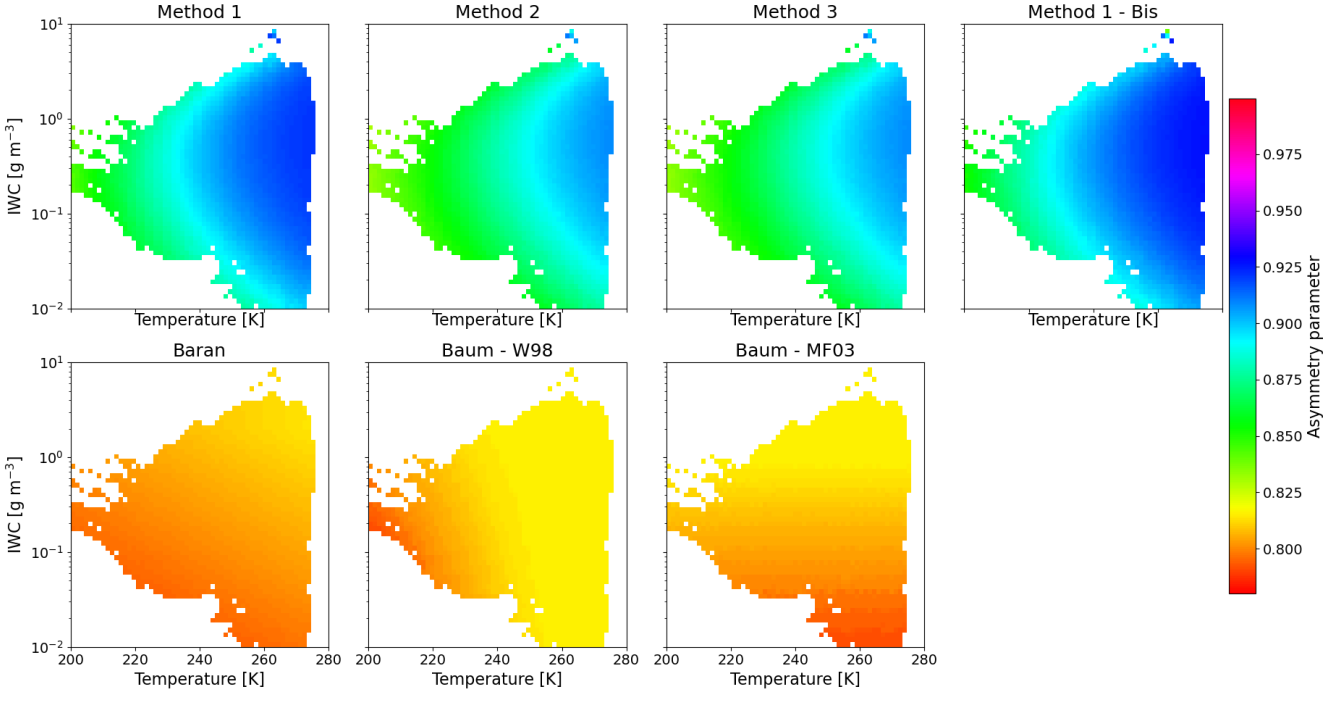

Figure 10. Comparison of asymmetry parameter given by the colorscale for the methods 1 to 3 and RTTOV parametrizations for 0.8 μm as a function of the temperature on y-axis and IWC on x-axis.

Figure 10 reveal several informations. First, it shows consistency with the phase functions (9), where all methods yield to relatively high asymmetry parameters (greater than 0.7, up to 0.95). The MF03 parametrization depend uniquely on the IWC

https://doi.org/10.5194/egusphere-2026-48
Preprint. Discussion started: 13 February 2026

and do not take temperature into account, as can be seen in these results. Our new methods propose asymmetry parameters between 0.86 and 0.92, which are higher than the ones in the parametrizations proposed by the RTTOV schemes (approximately 0.81). For the Baran and Baum W98 schemes, the dependence on temperature is low compare to the new methods. For our methods, the asymmetry parameter values are almost identical between the two spectral domains, while with RTTOV the value will be close to 1 in the infrared.

In summary, the analysis of extinction coefficients and phase functions illustrates the dependence of optical properties on both particle habit and spectral domain. Overall, these results show the optical properties of a specific case of an ice cloud originating from a tropical convective system characterized with high IWC. This leads to large values of both the extinction coefficient and the asymmetry parameter. However, some differences can be observed between all methods. These differences are expected to propagate into the radiative transfer simulations, directly influencing the simulated radiances.

3 Results

3.1 Simulations with RASTA retrievals

This section focuses on the results of the radiative transfer simulations performed using the different parametrizations presented before, which are compared with observations from MSG2/SEVIRI for each instrument channel. Figure 11 first presents a set of representative simulations. In this section, the results from Methods 2 and 3 are combined, as their differences are found to be negligible.

https://doi.org/10.5194/egusphere-2026-48
Preprint. Discussion started: 13 February 2026

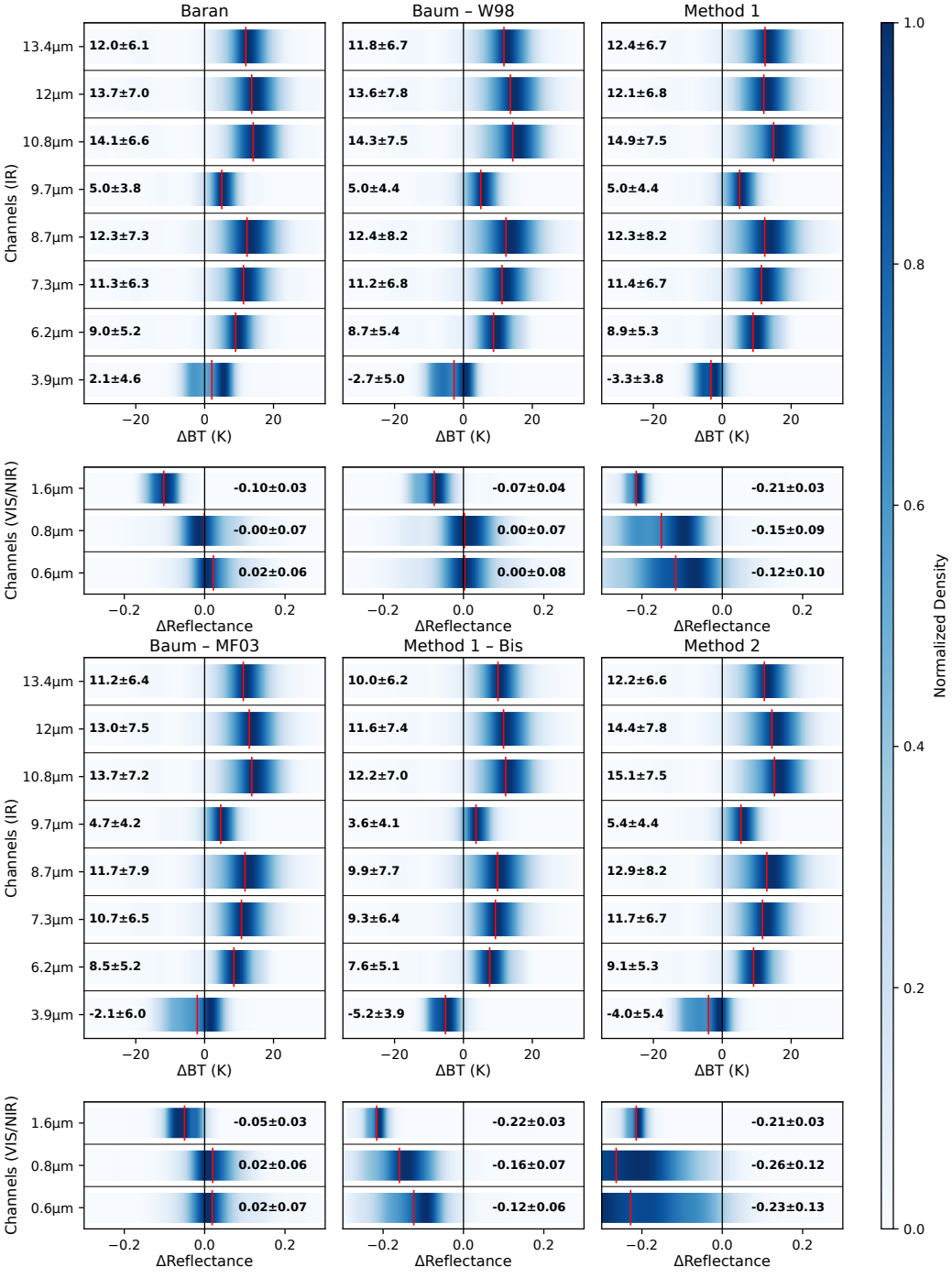

Figure 11. Top-view histogram of brightness temperature and reflectance differences (simulation with RTTOV minus observation of SEVIRI) for different methods. The red line indicates the mean and in black the value of the mean relative differences of reflectance (MRDR) and mean relative difference of simulated brightness temperatures (MRDTb) with their standard deviations.

https://doi.org/10.5194/egusphere-2026-48
Preprint. Discussion started: 13 February 2026

For these initial simulations, the distinction between the visible and infrared domains is noticeable.

In the infrared, for all methods and for all channels the mean relative difference of simulated brightness temperatures regarding the observed one (MRDTb) show a large positive bias exceeding +10 K ; except for the channel 3.9 μm and 9.7 μm with MRDTb about + 2.5 K and +5 K respectively. It indicates that our cloud tops appear systematically warmer than the one observed. Then, a misrepresentation of the cloud-top properties in the input data, since these channels are particularly sensitive to the upper layers of the cloud.

Note that, a difference of about 2 K is observed between Method 1 and Method 1-bis, highlighting the impact of the assumed PSD, in contrast with the much smaller differences (generally below 0.5 K) between Method 1 and Methods 2/3, which underlines the small influence of the assumed ice particle habit in the infrared for this case.

Thanks to these simulations we are suspecting an error in the estimation of IWC at the top of the cloud that can be explained by the sensitivity of the radar signal. Hence, the top of IWC profiles would be lower than the reality. In other we are missing information about the cloud tops. This could not have been countered with the combination of a lidar as we were flying in the cloud and not above as it is the case with the space missions (CloudSat/CALIPSO (Delanoë and Hogan, 2010)).

On the other side, for channels in the visible spectrum, there are two tendencies. First, the parametrizations from RTTOV provide small mean relative differences of reflectance (MRDR) with the observations for the 0.6 μm and 0.8 μm channels: 0.00 to 0.02. However, in the 1.6 μm channel, the MRDR increase to 0.05 and 0.1. Then, our new parametrizations show larger MRDR with the observations. The method 1 and method 1bis have similar reflectance error, by about 0.12, 0.15 and 0.21 in the channels 0.6 μm, 0.8 μm and 1.6 μm , respectively. While the method 2 and method 3 show very large MRDR of reflectance with the observations: more than 0.2 for the 3 visible channels.

In deep convective systems high reflectances are expected (Geiss et al., 2021). And the observed high reflectance can be attributed to a substantial IWC and strong solar irradiance, as the flight took place between 9:30 a.m. and 11:00 a.m. in the tropical region during summer. At 0.8 μm , reflectance values range from 0.8 to 0.9 and the comparison with Baum and Baran parametrization simulations shows good agreement in terms of mean and standard deviation.

https://doi.org/10.5194/egusphere-2026-48
Preprint. Discussion started: 13 February 2026

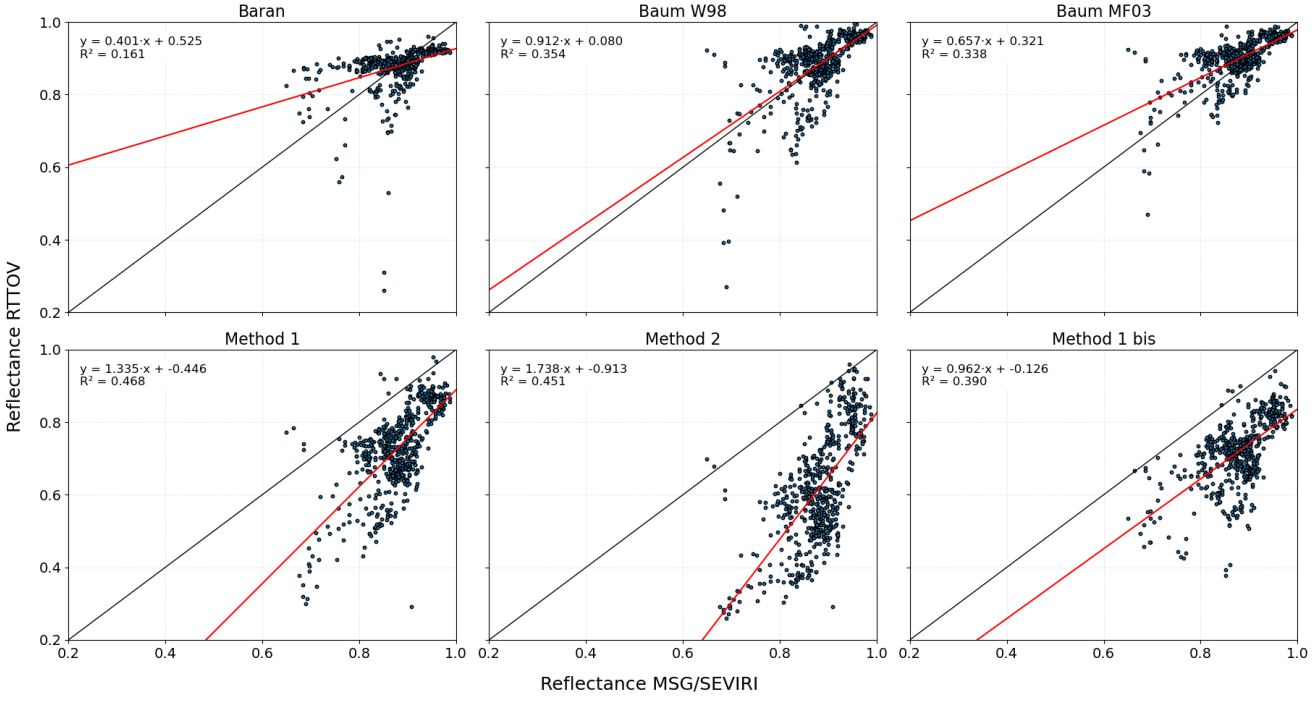

Figure 12. Correlation between simulation and observation for the channel 0,8μm, for the parametrization of RTTOV (Baran and Baum W98/MF03) and the new methods

The Figure 12 plots the reflectances for the 0.8 μm channel, observed with MSG2/SEVIRI versus the reflectances simulated with the different assumptions that we are using for our study. Despite a MRDR of 0.00 for the channel 0.8 μm (Figure 11), we can notice a bad correlation (R^2 = 0.161) between the simulated reflectance and the observed one, where a upper bound appears. Indeed, reflectance computed with the Baran parametrization tend to be around 0.9 (which is the most common reflectance observed by the satellite (Haney et al., 2023)). The most significant discrepancies appear where the RTTOV parametrizations predict lower reflectance, related with a lower asymmetry parameter (Figure 10). In contrast, the new methods tend to systematically underestimate reflectance. This discrepancy can be attributed to uncertainties in the particle size distribution and, above all, to the assumed ice crystal shapes. The difference between Methods 1 and 2 highlights the impact of the assumed particle habit. While Methods 1 and 1-bis the one of the PSD. Method 2 includes more complex crystal geometries (e.g., aggregates and bullet rosettes), which likely contribute to a lower reflectance under the same particle size distribution. With a significant bias, the correlation curve for method 1-bis appears to be the best (y = 0.952x -0.126).

3.2 Simulations with added cloud-top content

This section presents the results of RTTOV simulations in which additional IWC is introduced at the top of the retrieved IWC profiles. As discussed in the previous sections, this lack of IWC is suspected based on earlier results. To complete the retrieved IWC profiles, two parameters are required: the vertical limit up to which IWC can be added and the mean amount

https://doi.org/10.5194/egusphere-2026-48
Preprint. Discussion started: 13 February 2026

of ice introduced into the profiles. For the cloud tops, we use the 10.8 μm channel of MSG/SEVIRI. Indeed, this channel is a common indicator of cloud-top temperature for opac clouds (SMHI, 2021); the method assumes that the brightness temperature in this channel is related to the effective temperature at the cloud-top altitude.

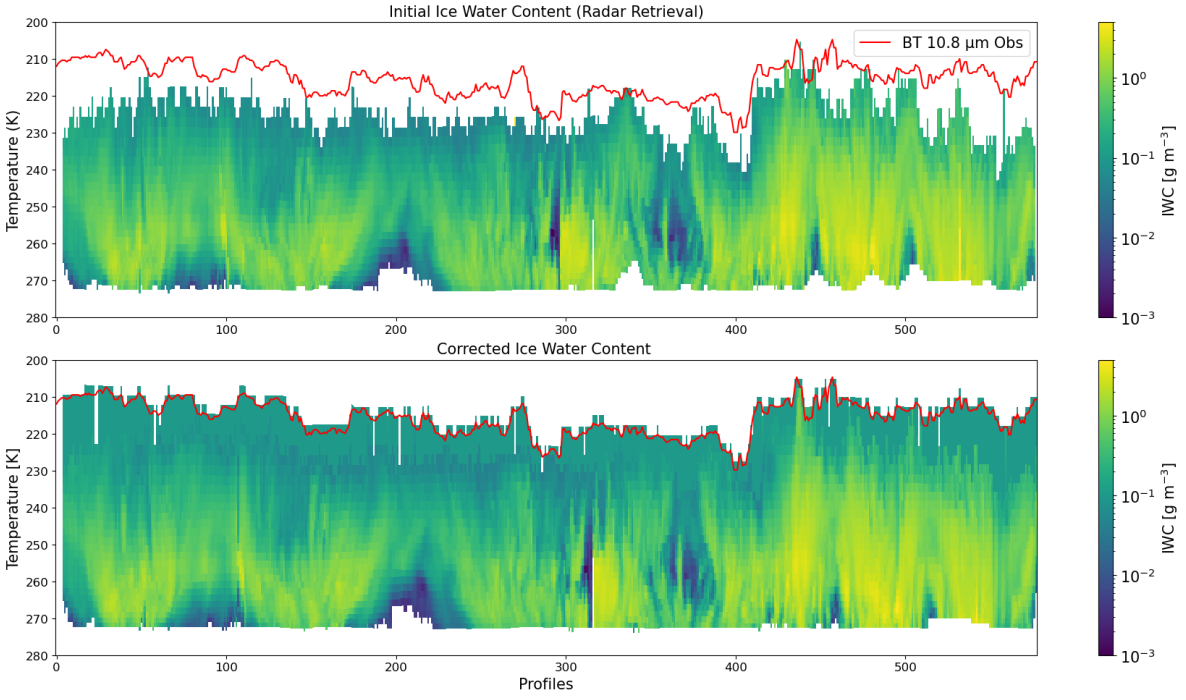

Figure 13. Complete IWC profiles with a content of $0.1\ \mathrm{g\,m^{-3}}$ based on the brightness temperature of the channel 10.8μm of MSG/SEVIRI

The new IWC profiles shown in Figure 13 were used to carry out new simulations. To determine the amount of content to be added to the upper layer, sensitivity tests were conducted with varying IWC. We found that the amount of $0.1\ \mathrm{g\,m^{-3}}$ significantly improved the simulations while maintaining a realistic concentration for an ice cloud top resulting from a convective system (Stein et al., 2024).

Building on the results from Figure 11, the same figure is now shown using the updated profiles with added cloud-top content:

https://doi.org/10.5194/egusphere-2026-48
Preprint. Discussion started: 13 February 2026

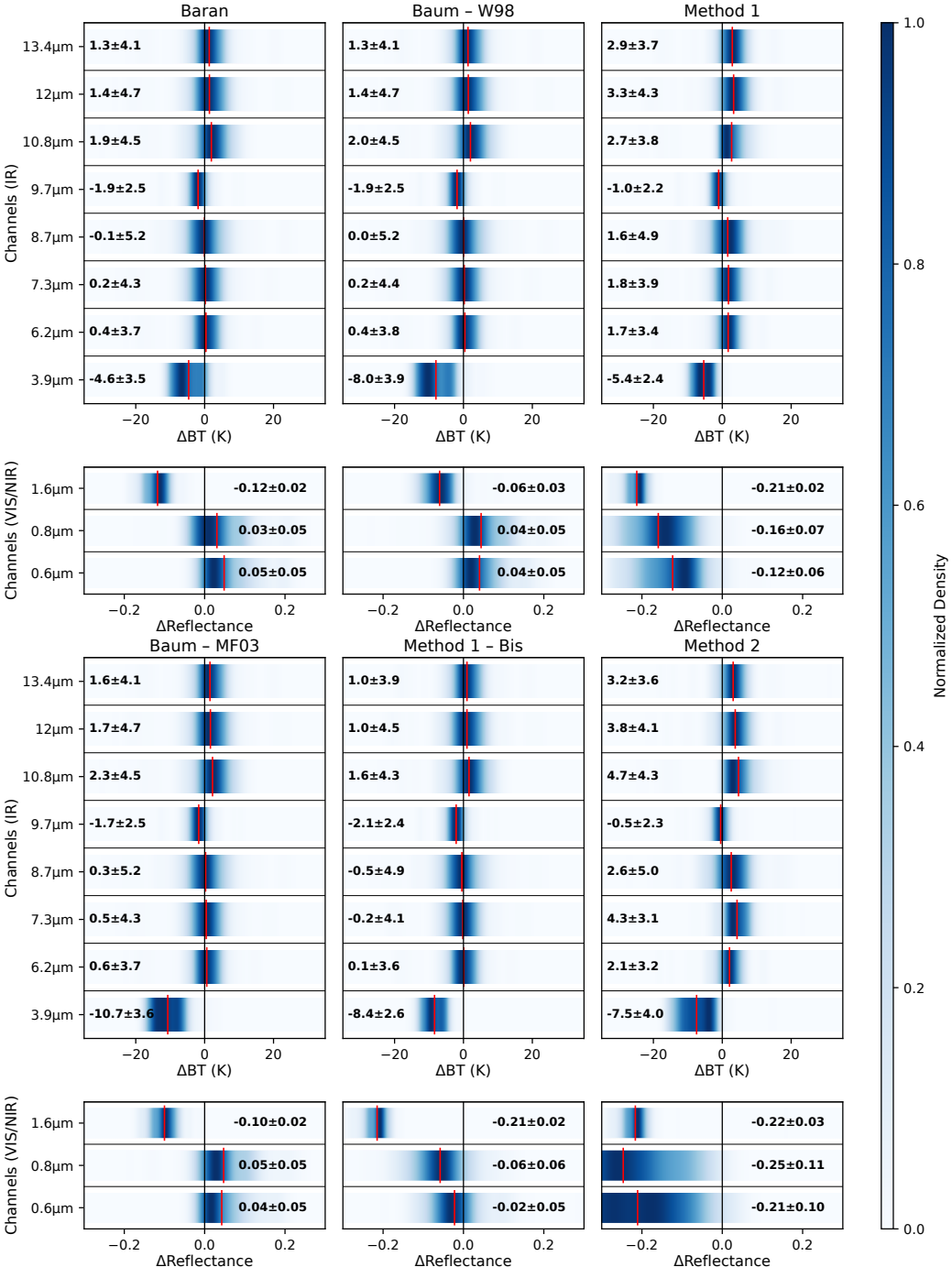

Figure 14. Same as figure 11, with adding a cloud top content of $0.1\ \mathrm{g\,m^{-3}}$

https://doi.org/10.5194/egusphere-2026-48
Preprint. Discussion started: 13 February 2026

As expected, the inclusion of additional IWC at the cloud top led to an improvement in the infrared simulations, reducing the MRDTb for all channels (not only the channel at 10.8 μm). For example, for the Baran parametrization and the 10.8 μm channel, the MRDTb decreases from 14 K to approximately 1.9 K, while for the 13.4 μm channel it decreases from 12 K to about 1.3 K. However, the sensitivity is different in the visible channels. For the RTTOV parametrizations (Baum and Baran), the MRDR is not significantly affected by the modification of IWC at cloud top. In contrast, Method 1bis, developed in this study, shows a significant decrease in MRDR for the 0.6 μm and 0.8 μm channels. With the corrected cloud-top IWC, Method 1bis exhibits MRDR values within the same range as those obtained with the RTTOV parametrizations. This is not the case for the other methods developed in this study (Methods 1, 2, and 3), despite their good performance in the infrared channel simulations. It is important to note that the only difference between Method 1 and Method 1bis lies in the PSD computation, based on Field et al. (2007) and Fontaine et al. (2020), respectively. Nevertheless, the 1.6 μm and 3.9 μm channels continue to exhibit inconsistent simulation results.

These results confirm that cloud-top IWC exerts a dominant control on simulated brightness temperatures but not on the reflectance. Also, reducing the concentration of small hydrometeors (< 100 μm) allowed us to improve the simulations of reflectance, bringing them closer to the observed one in the 0.6 and 0.8 μm channels. This reduces the bias between simulated and observed brightness temperatures by about 1 K, except for the 3.9 μm and 9.7 μm channels, for which the bias increases by few kelvins.

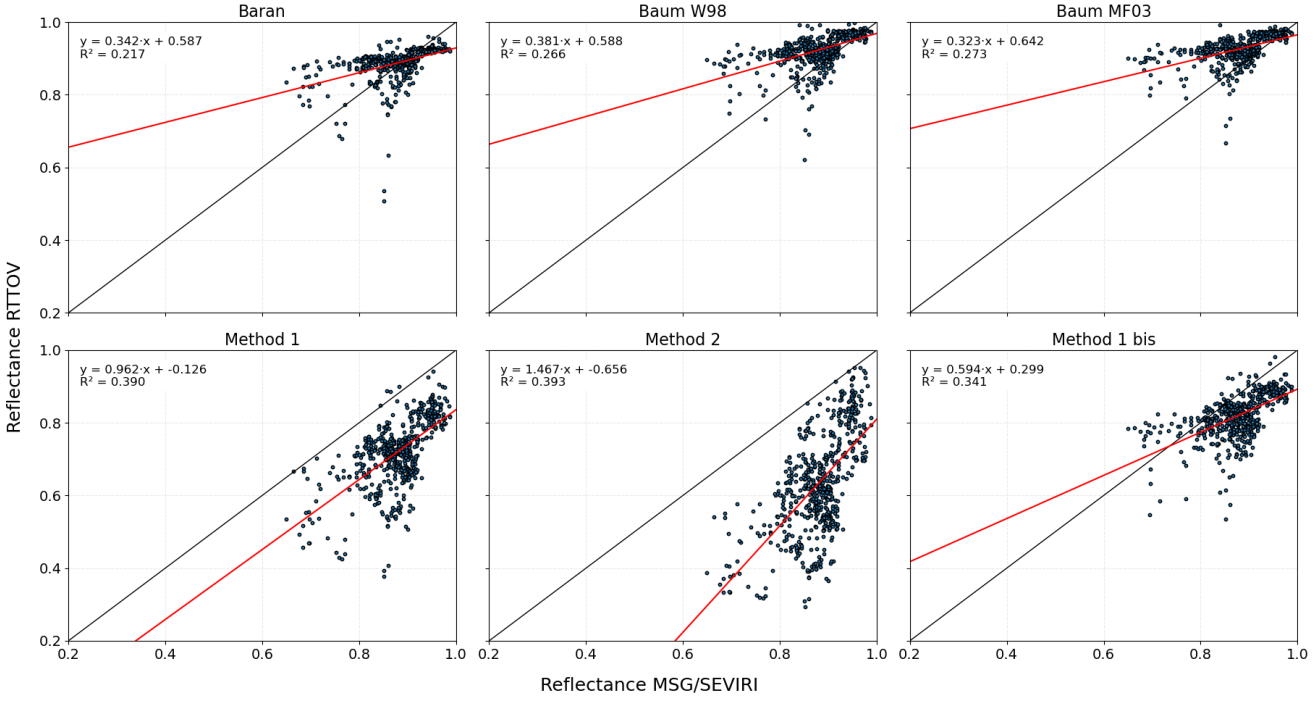

Figure 15. Same as Figure 12, with the new IWC profiles

https://doi.org/10.5194/egusphere-2026-48
Preprint. Discussion started: 13 February 2026

Figure 15 illustrates the results in the visible channel at 0.8 μm after correcting the retrieved IWC profiles. The correction of the IWC profiles increases the MRDR by a few percent for both the Baran and Baum parametrizations. However, for the Baum parametrization, this correction significantly alters the slope of the linear fit between the simulated and observed reflectances, leading to a decrease in the correlation between the two. In contrast, the correction has a substantial impact on the reflectances simulated using the parametrizations developed in this study. As mentioned earlier, it does not improve the simulated reflectances for Methods 1, 2, and 3, but only for Method 1bis. Nevertheless, the correction positively affects the correlation between simulations and observations for Method 1, while it negatively affects the correlation for Method 1bis.

This improvement in infrared simulations after adding IWC is due to the link between brightness temperatures and the altitude at which the cloud's radiation is completely attenuated. This implies that accurately simulating brightness temperatures requires two key parameters: (1) the cloud-top altitude and (2) the ice water path (IWP) integrated over a given cloud thickness. By contrast, the visible channels showed only small differences after cloud-top filling, demonstrating that reflectance is largely insensitive to small additions of high-altitude ice once the cloud optical depth exceeds a certain threshold.

4 Conclusions

The objective of this study is to evaluate the sensitivity of radiative transfer in visible and infrared channels regarding the distribution of ice crystals shapes in one deep convective cloud. We introduce new types of ice crystal shape distributions as a function of temperature and IWC, and compared their optical properties to three former parametrizations (Baran and Baum W98 and Baum MF03) developed for RTTOV. Hence, a series of reflectances and brightness temperatures simulations are performed for a case of a deep convective cloud during the West African Monsoon. This cloud was observed and sampled during the Megha-Tropiques airborne campaign in 2010 over Niamey. For this flight, IWC profiles were retrieved using the cloud radar RASTA. In the same time it was observed by the geostationary satellite MSG2/SEVIRI. Because this analysis is based on a single airborne case, the results primarily apply to convective systems exhibiting similar vertical structures and should not be generalized to all stages of deep convection.

Thanks to a first set of simulations, we highlight that IWC profiles at the top of the sampled cloud were truncated due to the sensitivity of the radar. In order to correct this, we assumed that the brightness temperature measured with MSG2/SEVIRI channel at 10.8 μm is a good estimation of the cloud top (black body assumption). Then, we filled the missing part of each IWC profiles with a constant amount of IWC of 0.1 $\mathrm{g\,m^{-3}}$. This correction allowed to improve the simulation in the infrared channels bringing brightness temperature closer to the observed ones, for all parametrization used here. However, it remains a mean bias of about +/- 1.5K to 2K for all these parametrizations. A key limitation of this study is that it relies on a single case study from the Megha-Tropiques campaign. Although this provides valuable insight into tropical deep convection, it restricts the generality of the conclusions. Moreover, uncertainties in radar-derived IWC—particularly introduce potential biases that cannot be fully quantified. Finally, the optical property schemes explored here remain sensitive to the assumed particle size distribution and mass–diameter relationships, which may not be representative of all convective regimes

https://doi.org/10.5194/egusphere-2026-48
Preprint. Discussion started: 13 February 2026

In the infrared, the results show a strong dependence on the vertical distribution of IWC, especially near the cloud top. The infrared simulation exposes the radar sensitivity and shows important information about what observation could miss at the top of the cloud. By adding an IWC of $0.1\ \mathrm{g\,m^{-3}}$ at the top of the cloud we reduce the bias between observation and simulation. This highlights the pronounced sensitivity of the infrared spectrum to high-altitude ice. And for convective clouds in the tropics, infrared channels will only observe the top of the cloud since the IWP is enough to fully attenuate the radiation.

In contrast, in the visible spectrum, ice clouds from convective system in the tropics are typically associated with very high reflectance, a feature reproduced by the simulations. However, the addition of small ice amounts at cloud top, while impactful in the infrared, has almost no big influence on reflectance. This behaviour reflects a saturation regime: once a certain optical depth is reached, further additions of ice have little effect on visible reflectances (Nakajima and King, 1990; Platnick, 2000). Thus, while the visible provides strong constraints on optical thickness, it is less informative on fine-scale variations in cloud-top IWC.

For satellite observations and retrieval applications, these findings carry informations. They confirm that the accuracy of brightness temperature simulations and consequently of ice cloud retrievals depends critically on a correct representation of both microphysics and vertical structure. In particular, window channels such as 10.8 μm are essential for constraining cloud-top temperature (Schmetz, 1993; Hamann et al., 2014). However, once optical saturation is reached, additional information on the internal vertical structure is lost. This underlines both the strength and the limitation of infrared observations: they are powerful probes of cloud-top properties, but cannot by themselves fully resolve the microphysical profile in case of thick ice cloud.

Finally, the alternative optical property schemes developed in this study did not systematically outperform the existing RTTOV parametrizations. Their limitations likely stem from residual inaccuracies in the assumed particle shapes or PSDs, which remain critical drivers of radiative properties. We shows that the particle shape and above all PSD have a strong impact to determine the optical properties (extinction coefficient or asymmetry parameter). In this particular cloud with a high IWC, PSD appears to be the most important factor for improving simulations. Nevertheless, the results confirm the importance of testing such approaches, as improved parametrizations may eventually help reduce systematic biases in cloud radiative transfer (Baran, 2012; Baum et al., 2014).

In summary, this work highlights the crucial role of cloud-top microphysics in shaping satellite observations. The infrared domain is especially sensitive to IWC at high altitude, while the visible primarily constrains total optical thickness. Accurate simulation of reflectances/brightness temperatures therefore requires both a robust representation of microphysical properties and careful treatment of cloud vertical structure. Although the proposed methods did not yet surpass the operational RTTOV schemes, the insights gained provide valuable guidance for future developments. Improved microphysical parametrizations, combined with better observational constraints, represent the next step toward more reliable use of radiative transfer models in both satellite retrievals and data assimilation contexts.

https://doi.org/10.5194/egusphere-2026-48
Preprint. Discussion started: 13 February 2026

Author contributions. RJ designed the study, developed the methodology, performed the simulations and analyses, and wrote the original manuscript. EF and JV supervised the overall work, contributed to the interpretation of the results, and reviewed and edited the manuscript. JD provided the dataset, supervised the methodological aspects related to the data, and contributed to the interpretation of the results.

Competing interests. The authors declare that they have no conflict of interest.

Acknowledgements.

https://doi.org/10.5194/egusphere-2026-48
Preprint. Discussion started: 13 February 2026

References

Baek, S.-J., Yang, P., Baum, B. A., King, M. D., Nasiri, S. L., and Heidinger, A. K.: New optical properties of ice crystals for shortwave radiative transfer studies, Journal of Advances in Modeling Earth Systems, 10, 981–1002, https://doi.org/10.1002/2017MS001180, 2018.

Baran, A., Cotton, R., Furtado, K., Havemann, S., C.-Labonnote, L., Marenco, F., Smith, A., and Thelen, J.-C.: A self-consistent scattering model for cirrus. II: The high and low frequencies, Quarterly Journal of the Royal Meteorological Society, 140, https://doi.org/10.1002/qj.2193, 2014.

Baran, A. J.: A review of the light scattering properties of cirrus, Journal of Quantitative Spectroscopy and Radiative Transfer, 110, 1239–1260, https://doi.org/10.1016/j.jqsrt.2009.02.026, 2009.

Baran, A. J.: From the single-scattering properties of ice crystals to climate prediction: A way forward, Atmospheric Research, 112, 45–69, https://doi.org/10.1016/j.atmosres.2012.04.010, 2012.

Baum, B. A., Heymsfield, A. J., Yang, P., and Bedka, S. T.: Bulk Scattering Properties for the Remote Sensing of Ice Clouds. Part I: Microphysical Data and Models, Journal of Applied Meteorology, 44, 1885–1895, https://doi.org/10.1175/JAM2308.1, 2005.

Baum, B. A., Yang, P., Heymsfield, A. J., Schmitt, C. G., Xie, Y., Bansemer, A., Hu, Y.-X., and Zhang, Z.: Improvements in Shortwave Bulk Scattering and Absorption Models for the Remote Sensing of Ice Clouds, Journal of Applied Meteorology and Climatology, 50, 1037–1056, https://doi.org/10.1175/2010JAMC2608.1, 2011.

Baum, B. A., Yang, P., Heymsfield, A. J., Bansemer, A., Hu, Y.-X., et al.: Ice cloud single-scattering property models with the full phase matrix at wavelengths from 0.2 to 100 μm, Journal of Quantitative Spectroscopy and Radiative Transfer, 146, 123–139, https://doi.org/10.1016/j.jqsrt.2014.02.029, 2014.

Bohren, C. F. and Huffman, D. R.: Absorption and Scattering of Light by Small Particles, 1 edn., ISBN 978-0-471-29340-8 978-3-527-61815-6, https://doi.org/10.1002/9783527618156, 1998.

Bojanowski, J. S., Stöckli, R., Tetzlaff, A., and Kunz, H.: The Impact of Time Difference between Satellite Overpass and Ground Observation on Cloud Cover Performance Statistics, Remote Sensing, 6, 12 866–12 884, https://doi.org/10.3390/rs61212866, 2014.

Bony, S., Stevens, B., Frierson, D. M. W., Jakob, C., Kageyama, M., Pincus, R., Shepherd, T. G., and Sherwood, S. C.: Clouds, circulation and climate sensitivity, Nature Geoscience, 8, 261–268, https://doi.org/10.1038/ngeo2398, 2015.

Cole, B. H., Yang, P., Baum, B. A., Riedi, J., and C.-Labonnote, L.: Ice particle habit and surface roughness derived from PARASOL polarization measurements, Atmospheric Chemistry and Physics, 14, 3739–3750, https://doi.org/10.5194/acp-14-3739-2014, 2014.

Cotton, R. J., Field, P. R., Ulanowski, Z., Kaye, P. H., Hirst, E., Greenaway, R. S., Crawford, I., Crosier, J., and Dorsey, J.: The effective density of small ice particles obtained from *in situ* aircraft observations of mid-latitude cirrus: Effective Density of Small Ice Particles, Quarterly Journal of the Royal Meteorological Society, 139, 1923–1934, https://doi.org/10.1002/qj.2058, 2013.

Delanoë, J. and Hogan, R. J.: A variational scheme for retrieving ice cloud properties from combined radar, lidar and infrared radiometer, Journal of Geophysical Research, 113, D07 204, https://doi.org/10.1029/2007JD009000, 2008.

Delanoë, J. and Hogan, R. J.: Combined CloudSat-CALIPSO-MODIS retrievals of the properties of ice clouds, Journal of Geophysical Research: Atmospheres, 115, https://doi.org/10.1029/2009JD012346, 2010.

Delanoë, J. M. E., Heymsfield, A. J., Protat, A., Bansemer, A., and Hogan, R. J.: Normalized Particle Size Distribution for Remote Sensing Application, Journal of Geophysical Research: Atmospheres, 119, 4204–4227, https://doi.org/10.1002/2013JD020700, 2014.

Dolinar, E. K., Paciorek, C. J., Clair, C. A. S., and Weaver, C. P.: Perspectives on Cloud Prediction, Postprocessing, and Assimilation, Bulletin of the American Meteorological Society, 105, E1255–E1272, https://doi.org/10.1175/BAMS-D-24-0077.1, 2024.

https://doi.org/10.5194/egusphere-2026-48
Preprint. Discussion started: 13 February 2026

Drigeard, E., Fontaine, E., Wobrock, W., Schwarzenbock, A., Duroure, C., Williams, E. R., Russell, B., Protat, A., Delanoe, J., Cazenave, F., and Gosset, M.: A Comparison of Airborne In Situ Cloud Microphysical Measurement with Ground-Based C-Band Radar Observations in Deep Stratiform Regions of African Squall Lines, Journal of Applied Meteorology and Climatology, 54, 2461–2477, https://doi.org/10.1175/JAMC-D-14-0262.1, 2015.

Duncan, D. I. and Eriksson, P.: An update on global atmospheric ice estimates from satellite observations and reanalyses, Atmospheric Chemistry and Physics, 18, 11 205–11 219, https://doi.org/10.5194/acp-18-11205-2018, 2018.

Field, P. R., Heymsfield, A. J., and Bansemer, A.: Snow Size Distribution Parameterization for Midlatitude and Tropical Ice Clouds, Journal of the Atmospheric Sciences, 64, 4346–4365, https://doi.org/10.1175/2007JAS2344.1, publisher: American Meteorological Society Section: Journal of the Atmospheric Sciences, 2007.

Fontaine, E., Schwarzenboeck, A., Leroy, D., Delanoë, J., Protat, A., Dezitter, F., Strapp, J. W., and Lilie, L. E.: Statistical analysis of ice microphysical properties in tropical mesoscale convective systems derived from cloud radar and in situ microphysical observations, Atmospheric Chemistry and Physics, 20, 3503–3553, https://doi.org/10.5194/acp-20-3503-2020, 2020.

Fridlind, A. M. et al.: High ice water content at low reflectivity – Part 1, Atmospheric Chemistry and Physics Discussions, 15, 16 505–16 550, https://doi.org/10.5194/acpd-15-16505-2015, 2015.

Geer, A. J., Lonitz, K., Weston, P., Kazumori, M., Okamoto, K., Zhu, Y., Liu, E. H., Collard, A., Bell, W., Migliorini, S., et al.: All-sky satellite data assimilation at operational weather forecasting centres, Quarterly Journal of the Royal Meteorological Society, https://doi.org/10.1002/qj.3202.

Geiss, S., Scheck, L., de Lozar, A., and Weissmann, M.: Understanding the model representation of clouds based on visible and infrared satellite observations, Atmospheric Chemistry and Physics, 21, 12 273–12 290, https://doi.org/10.5194/acp-21-12273-2021, 2021.

Hamann, U., Walther, A., Baum, B., Bennartz, R., Bugliaro, L., Derrien, M., Francis, P. N., Heidinger, A., Joro, S., Kniffka, A., Le Gléau, H., Lockhoff, M., Lutz, H.-J., Meirink, J. F., Minnis, P., Palikonda, R., Roebeling, R., Thoss, A., Platnick, S., Watts, P., and Wind, G.: Remote sensing of cloud top pressure/height from SEVIRI: analysis of ten current retrieval algorithms, Atmospheric Measurement Techniques, 7, 2839–2867, https://doi.org/10.5194/amt-7-2839-2014, publisher: Copernicus GmbH, 2014.

Haney, C. O., Doelling, D. R., Bhatt, R., Khakurel, P., Scarino, B., and Gopalan, A.: The impact of pixel size on the characterization of deep convective clouds for calibration, Proceedings of SPIE, Earth Observing Systems XXVIII, 12678, 126 780I, https://doi.org/10.1117/12.2677709, 2023.

Key, J. R., Yang, P., Baum, B. A., and Nasiri, S. L.: Parameterization of shortwave ice cloud optical properties for various particle habits, Journal of Geophysical Research: Atmospheres, 107, https://doi.org/10.1029/2001JD000742, 2002.

Korolev, A., Qu, Z., Milbrandt, J., Heckman, I., Cholette, M., Wolde, M., Nguyen, C., McFarquhar, G. M., Lawson, P., and Fridlind, A. M.: High ice water content in tropical mesoscale convective systems (a conceptual model), Atmospheric Chemistry and Physics, 24, 11 849–11 881, https://doi.org/10.5194/acp-24-11849-2024, 2024.

Liou, K.-N.: Influence of Cirrus Clouds on Weather and Climate Processes: A Global Perspective, Monthly Weather Review, 114, 1167–1199, https://doi.org/10.1175/1520-0493(1986)114<1167:IOCCOW>2.0.CO;2, publisher: American Meteorological Society Section: Monthly Weather Review, 1986.

Liou, K. N.: An Introduction to Atmospheric Radiation, vol. 84 of *International Geophysics*, San Diego, 2 edn., 2002.

Massie, S., Gettelman, A., Randel, W., and Baumgardner, D.: Distribution of tropical cirrus in relation to convection, Journal of Geophysical Research: Atmospheres, 107, https://doi.org/10.1029/2001JD001293, 2002.

https://doi.org/10.5194/egusphere-2026-48
Preprint. Discussion started: 13 February 2026

Masson-Delmotte, V., Zhai, P., Pirani, A., Connors, S. L., Péan, C., Berger, S., Caud, N., Chen, Y., Goldfarb, L., Gomis, M. I., Huang, M., Leitzell, K., Lonnoy, E., Matthews, J. B. R., Maycock, T. K., Waterfield, T., Yelekçi, O., Yu, R., and Zhou, B., eds.: Climate Change 2021: The Physical Science Basis, Cambridge, United Kingdom and New York, NY, USA, https://doi.org/10.1017/9781009157896, 2021.

McFarquhar, G. M., Iacobellis, S., and Somerville, R. C. J.: Single-column model simulations of tropical ice clouds using observationally based parameterizations of microphysics, Journal of Climate, 16, 1643–1664, https://doi.org/10.1175/1520-0442(2003)016<1643:SMSOTI>2.0.CO;2, 2003.

Mishchenko, M. I., Travis, L. D., and Mackowski, D. W.: T-matrix computations of light scattering by nonspherical particles: A review, Journal of Quantitative Spectroscopy and Radiative Transfer, 55, 535–575, https://doi.org/10.1016/0022-4073(96)00002-7, 1996.

Nakajima, T. and King, M. D.: Determination of the Optical Thickness and Effective Particle Radius of Clouds from Reflected Solar Radiation Measurements. Part I: Theory, Journal of the Atmospheric Sciences, 47, 1878–1893, https://doi.org/10.1175/1520-0469(1990)047<1878:DOTOTA>2.0.CO;2, 1990.

Okamoto, K., Ishibashi, T., and Okabe, I.: All-sky infrared radiance assimilation of a geostationary satellite in the Japan Meteorological Agency's global system, Quarterly Journal of the Royal Meteorological Society, 149, 2477–2503, https://doi.org/10.1002/qj.4516, _eprint: https://onlinelibrary.wiley.com/doi/pdf/10.1002/qj.4516, 2023.

Platnick, S.: Vertical photon transport in cloud remote sensing problems, Journal of Geophysical Research: Atmospheres, 105, 22 919–22 935, https://doi.org/10.1029/2000JD900333, 2000.

Protat, A., Bouniol, D., Delanoë, J., O'Connor, E., May, P. T., Plana-Fattori, A., Hasson, A., Görsdorf, U., and Heymsfield, A. J.: Assessment of CloudSat Reflectivity Measurements and Ice Cloud Properties Using Ground-Based and Airborne Cloud Radar Observations, Journal of Atmospheric and Oceanic Technology, 26, 1717–1741, https://doi.org/10.1175/2009JTECHA1246.1, 2009.

Protat, A., Rauniyar, S., Delanoë, J., Fontaine, E., and Schwarzenboeck, A.: W-Band (95 GHz) Radar Attenuation in Tropical Stratiform Ice Anvils, Journal of Atmospheric and Oceanic Technology, 36, 1463–1476, https://doi.org/10.1175/JTECH-D-18-0154.1, 2019.

Pujol, O., Georgis, J.-F., Féral, L., and Sauvageot, H.: Degradation of Radar Reflectivity by Cloud Attenuation at Microwave Frequency, Journal of Atmospheric and Oceanic Technology, 24, 640–657, https://doi.org/10.1175/JTECH1992.1, 2007.

Rädel, G., Shine, K. P., and Stuber, N.: Radiative forcing by persistent contrails and its dependence on cruise altitudes, Journal of Geophysical Research: Atmospheres, 113, D07 105, https://doi.org/10.1029/2007JD009117, 2008.

Roca, R., Brogniez, H., Chambon, P., Chomette, O., Cloche, S., Gosset, M. E., Mahfouf, J.-F., Raberanto, P., and Viltard, N.: The Megha-Tropiques mission: a review after three years in orbit, Frontiers in Earth Science, 3, 17, https://doi.org/10.3389/feart.2015.00017, 2015.

Saunders, R., Lupu, C., Hocking, J., Turner, E., Rayer, P., Rundle, D., Brunel, P., Vidot, J., Roquet, P., Matricardi, M., Geer, A., and Bormann, N.: An update on the RTTOV fast radiative transfer model (currently at version 12), https://doi.org/https://doi.org/10.5194/gmd-11-2717-2018, 2018.

Schmetz, J.: Operational cloud-motion winds from Meteosat infrared images, Monthly Weather Review, 121, 1206–1215, https://doi.org/10.1175/1520-0493(1993)121<1206:OCMWFM>2.0.CO;2, 1993.

Schmetz, J., Pili, P., Tjemkes, S., Just, D., Kerkmann, J., Rota, S., and Ratier, A.: An Introduction to Meteosat Second Generation (MSG), Bulletin of the American Meteorological Society, 83, 977–992, https://doi.org/10.1175/1520-0477(2002)083<0977:AITMSG>2.3.CO;2, 2002.

Schmitt, C. G. and Heymsfield, A. J.: Observational quantification of the separation of simple and complex atmospheric ice particles, Journal of the Atmospheric Sciences, 71, 2594–2609, https://doi.org/10.1175/JAS-D-13-0134.1, 2014.

https://doi.org/10.5194/egusphere-2026-48
Preprint. Discussion started: 13 February 2026

Schmitt, C. G., Heymsfield, A. J., Connolly, P., Järvinen, E., and Schnaiter, M.: A Global View of Atmospheric Ice Particle Complexity, Geophysical Research Letters, 43, https://doi.org/10.1002/2016GL071267, 2016.

SMHI: Algorithm Theoretical Basis Document for Cloud Top Temperature, Pressure and Height of the NWC/PPS, Tech. Rep. NWC/CDOP3/PPS/SMHI/SCI/ATBD/CTTH, NWC SAF, https://www.nwcsaf.org/Downloads/PPS/v2021/Documents/NWC-CDOP3-PPS-SMHI-SCI-ATBD-CTTH_v3_0.pdf, 2021.

Stein, T. H., Illingworth, A. J., Hogan, R. J., Cornet, C., Protat, F., Protat, A., and Grandin, A.: High ice water content in tropical mesoscale convective systems (a conceptual model), Atmospheric Chemistry and Physics, 24, 11 849–11 881, https://doi.org/10.5194/acp-24-11849-2024, 2024.

Stubenrauch, C. J., Rossow, W. B., Kinne, S., Ackerman, S., Cesana, G., Chepfer, H., Di Girolamo, L., Getzewich, B., Guignard, A., Heidinger, A., Maddux, B. C., Menzel, W. P., Minnis, P., Pearl, C., Platnick, S., Poulsen, C., Riedi, J., Sun-Mack, S., Walther, A., Winker, D., Zeng, S., and Zhao, G.: Assessment of Global Cloud Datasets from Satellites: Project and Database Initiated by the GEWEX Radiation Panel, Bulletin of the American Meteorological Society, 94, 1031–1049, https://doi.org/10.1175/BAMS-D-12-00117.1, 2013.

Vidot, J., Baran, A. J., and Brunel, P.: A new ice cloud parameterization for infrared radiative transfer simulation of cloudy radiances: Evaluation and optimization with IIR observations and ice cloud profile retrieval products, Journal of Geophysical Research: Atmospheres, 120, 6937–6951, https://doi.org/10.1002/2015JD023462, 2015.

Wang, C., Yang, P., Nasiri, S. L., Baum, B. A., Platnick, S., and Heidinger, A. K.: Retrieval of ice cloud properties using an optimal estimation algorithm and MODIS infrared observations, Journal of Geophysical Research: Atmospheres, 121, 5809–5826, https://doi.org/10.1002/2015JD024528, 2016.

Wylie, D. P. and Menzel, W. P.: Eight Years of High Cloud Statistics Using HIRS, Journal of Climate, 12, 170–184, https://doi.org/10.1175/1520-0442(1999)012<0170:EYOHCS>2.0.CO;2, publisher: American Meteorological Society Section: Journal of Climate, 1999.

Wyser, K.: The effective radius in ice clouds, Journal of Climate, 11, 1793–1802, https://doi.org/10.1175/1520-0442(1998)011<1793:TERIIC>2.0.CO;2, 1998.

Yang, P., Bi, L., Baum, B. A., Liou, K.-N., Kattawar, G. W., Mishchenko, M. I., and Cole, B.: Spectrally Consistent Scattering, Absorption, and Polarization Properties of Atmospheric Ice Crystals at Wavelengths from 0.2 to 100 μm, Journal of the Atmospheric Sciences, 70, 330–347, https://doi.org/10.1175/JAS-D-12-039.1, 2013.

Zhu, L., Li, S., Ma, Z., Wang, H., and Yin, Y.: Impact of Cloud Microphysics Initialization Using Satellite Data, Remote Sensing, 17, 2507, https://doi.org/10.3390/rs17142507, 2025.